soluble aggregates/inclusion bodies [19-23]. Although it is still unclear which intermediate species are responsible for polyQ disease pathogenesis, these facts indicate that the expanded polyQ protein gains cytotoxicity during the aggregation process.

THERAPEUTIC APPROACHES FOR THE POLYGLUTAMINE DISEASES

Since proteins with an abnormally expanded polyQ stretch gain cytotoxicity during their aggregation process, suppression of misfolding and aggregate formation could be a potential therapeutic approach for treatment of the polyQ diseases [3]. Several studies have actually demonstrated in polyQ disease models that increasing levels of molecular chaperones [24-28] and expression of intracellular antibodies (intrabodies) [29-31] successfully reduce the eventual toxicity in neurons through suppression of polyQ protein accumulation and inclusion body formation [32, 33]. Small molecules [34-38] and peptides [39-41] that interfere with the aggregation process of the expanded polyQ protein were also shown to suppress polyQ-induced neurodegeneration in cell culture and animal models of the polyQ diseases. In addition, activation of protein degradation systems, which accelerate the clearance of the polyQ proteins, has been shown to be quite effective to suppress aggregate formation and eventual cell death [42,43]. Since suppression of polyQ aggregation is expected to broadly correct the functional abnormalities of multiple downstream cellular processes (see below), misfolding and aggregate formation of the expanded polyQ proteins are one of the most ideal therapeutic targets of the polyQ diseases [3] (Fig. **1**).

On the other hand, it is well known that polyQ disease patients as well as animal models exhibit dysfunctions in various cellular processes in the cascade of polyQ pathogenesis. This includes abnormalities in essential cellular functions including transcription [44], proteasomal degradation [45], synaptic transmission [46], axonal transport [47] and Ca^{2+} signaling pathways [48], which probably contribute to neuronal dysfunction and eventual loss of neurons in various regions of the brain [12, 49, 50]. Although the exact mechanisms as to how they eventually cause degeneration of neurons in patients of the polyQ diseases have not yet been clarified, these cellular processes that are thought to be eventually impaired in the pathogenic cascade are also potential therapeutic targets for treatment of the polyQ diseases (Fig. **1**).

In the following sections, selected examples of peptide-based therapeutic approaches focusing on these targets are introduced (Table **1**), and the current problems that must be overcome for the development of peptide-based therapies for the polyQ diseases are discussed.

PEPTIDE-BASED INHIBITORS OF POLYGLUTAMINE AGGREGATION

Therapeutic approaches targeting the polyQ stretch are particularly attractive because effective inhibitors would be expected to work generally on a broad spectrum of the polyQ diseases. Trottier *et al.* showed that the anti-polyQ monoclonal antibody 1C2 binds preferentially to longer polyQ repeats compared with short repeats [51]. Similar preferential binding to expanded polyQ proteins has been reported for the monoclonal antibodies MW1 [52] and 3B5H10 [53]. These studies led to the idea that expanded polyQ stretches may possess structurally different conformations from the shorter ones, and that potential molecules that specifically recognize and bind to such abnormal conformations could interfere with the aggregation processes of expanded polyQ proteins.

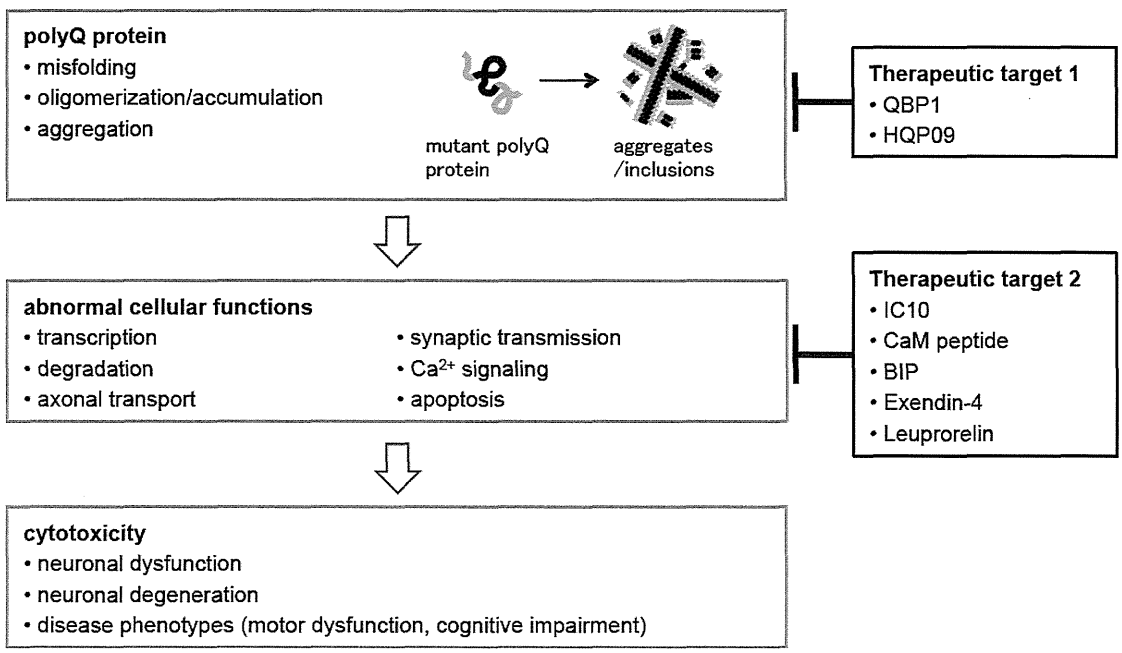

Fig. (1). Proposed mechanism of expanded polyQ protein toxicity and potential therapeutic targets for polyQ disease therapies.

Table 1. Selected examples of peptides potentially effective for the polyQ diseases.

Peptide	Sequence	Therapeutic Target	Effects *In Vitro*	Effects *In Vivo*	Ref
QBP1	SNWKWWPGIFD	polyQ aggregation	Aggregation ↓ Inclusion bodies ↓ Cytotoxicity ↓	Inclusion bodies ↓ Life span ↑ Body weight ↑	[23, 39, 54-60, 62, 63]
HQP09	Npip-Nmba-P-Nmea-Nall-Nlys-Nser[a]	polyQ aggregation	Aggregation ↓ Cytotoxicity ↓	Stabilize Ca^{2+} signaling ↓ Apoptosis ↓ Inclusion bodies	[64]
IC10	A cytosolic C-terminal tail of $InsP_3R1$ (122 amino acids)	Aberrant interaction between Htt and $InsP_3R1$	Stabilize Ca^{2+} signaling ↓	Motor function ↑ Neuronal loss ↓	[68]
CaM peptide	MKDTDSEEEIREAFRVFDKDGNGY-ISAAELRHVMTNLGEKLTDEEV (A fragment of CaM, residues 76-121)	Abberant interaction between Htt and CaM	Cytotoxicity ↓	Body weight ↑ Motor function ↑ Inclusion bodies ↓	[69-71]
BIP	VPMLK/VPTLK	Bax-induced apoptosis	Apoptosis ↓	-	[75,76]
Exendin-4	HGEGTFTSDLSKQMEEEAVRLFIEWL KNGGPSSGAPPPS	Abnormal energy metabolism	-	Motor function ↑ Life span ↑ Inclusion bodies ↓	[85]
Leuprorelin	Pyr-HWSY*L*LRP-NHEt[b,c]	Nuclear accumulation of mutant AR	-	Motor function ↑ Life span ↑ Inclusion bodies ↓	[90-92]

[a]N-substituted glycines. Npip, piperonyl; Nmba, methylbenzyl; Nmea, methoxyethyl; Nall, allyl; Nlys, aminobutyl; Nser, hydroxyethyl. [b]Pyr, pyroglutamyl. [c]*d*-amino acids in *Italics*.

QBP1

We previously took a combinatorial screening approach to search for short peptides that selectively and specifically bind to an expanded polyQ stretch, but not to a normal length polyQ stretch, using the phage display technique. Multiple rounds of screening resulted in six peptides that preferentially bind to the abnormally expanded polyQ stretch [39]. One of these peptides, QBP1 (polyQ binding peptide 1), had a particularly high affinity for the abnormal polyQ stretch with a dissociation constant (K_d) of 5.7 μM [54], and also had a suppressive effect on polyQ aggregation *in vitro* [39]. Studies focusing on its structure-activity relationship revealed that the tryptophan-rich sequence is necessary for the inhibitory activity of QBP1 [55-57]. Expression of QBP1 effectively suppressed inclusion body formation and cytotoxicity of expanded polyQ proteins in cell culture [23,39,58,59] and *Drosophila* models of the polyQ diseases [60]. Since QBP1 is poorly membrane permeable, we employed protein transduction domains (PTDs) [61] to improve the bioavailability of QBP1 by its efficient intracellular delivery. We found that the delivery efficiency of QBP1 was dramatically improved by conjugation with a PTD, leading to successful suppression of polyQ inclusions as well as polyQ-induced premature death in *Drosophila* by its oral administration [62]. The therapeutic potential of PTD-QBP1 was further investigated using a mouse model of HD. However, the therapeutic effect of PTD-QBP1 was limited to neither inhibition of body weight loss with any improvement in the other disease phenotypes nor inhibition of aggregate formation in the brains, probably due to low efficiency of PTD-QBP1 delivery to the mouse brain by intraperitoneal injections [63].

HQP09

Chen *et al.* also performed combinatorial screening to search for potential inhibitors of polyQ aggregation [64]. In contrast to our approach using peptide-based phage display libraries, they used a combinatorial library consisting of peptoids as scaffolds. Peptoids, which are oligomers of N-substituted glycines, have an advantage in developing therapeutic molecules since they are considered to be superior in stability to protease degradation, cell permeability, and structural diversity [65, 66]. They prepared a peptoid library containing 60,000 unique compounds, and screened for molecules that specifically bind to the Htt fragment with an expanded polyQ stretch. The peptoid HQP09, which was isolated from this screening process, was found to bind with high specificity to the expanded polyQ forms of Htt and ataxin-3, which is the causative protein of SCA3, and to effectively suppress polyQ aggregation *in vitro*. Interestingly, although HQP09 and QBP1 had comparable binding affinity to mutant Htt proteins, HQP09 did not show any competition with QBP1 in binding, possibly indicating that these two inhibitors recognize the abnormally expanded polyQ stretches in a different manner. The authors also tested the therapeutic activity of this peptoid, and confirmed that HQP09 reduced cytotoxicity in primary cultured neurons and decreased polyQ inclusion bodies in a mouse model of HD upon its intracerebroventricular injection. Importantly, they successfully identified the pharmacophore of HQP09 based on a structure-activity relationship study, and developed the minimal derivative peptoid HQP09-9 (4-mer, MW = 585) without significant loss of activity. Although HQP09-9 failed to exert therapeutic effects on a mouse model upon its subcu-

taneous injection probably due to poor blood-brain barrier permeability, this could be a promising lead compound for the development of drugs against a broad spectrum of the polyQ diseases.

PEPTIDE-BASED MODULATORS OF POLYGLUTAMINE TOXICITY

Another therapeutic approach is to target the various cellular dysfunctions occurring in the cascade of polyQ pathogenesis. Although the mechanisms as to how these abnormalities contribute to eventual neurodegeneration in various regions of the brain are not known, normalizing such dysfunctions has been shown to effectively reduce the toxicity of the expanded polyQ proteins and improve disease phenotypes in polyQ disease animal models.

IC10 peptide

Since aberrant interactions between mutant Htt and various proteins often cause abnormalities in downstream cellular functions [50], disruption of such interactions could be a promising therapeutic approach. Bezprozvanny and coworkers found that the polyQ expanded Htt protein specifically binds to type 1 inositol 1,4,5-triphosphate receptor ($InsP_3R1$) and facilitates its activity, indicating that abnormal neuronal Ca^{2+} signaling may play an important role in HD pathogenesis [48, 67]. Since mutant Htt specifically binds to the C-terminal cytosolic region of $InsP_3R1$ (IC10 fragment), they hypothesized that introduction of the IC10 peptide into neurons would normalize Ca^{2+} signaling and eventual neurodegeneration by interfering with the abnormal interaction between mutant Htt and $InsP_3R1$[48]. They indeed found that viral vector-mediated expression of the IC10 peptide effectively stabilized neuronal Ca^{2+} signaling, improved motor dysfunctions and reduced neuronal loss in a mouse model of HD [68].

CaM-peptide

Mutant Htt also associates with calmodulin (CaM) with a higher affinity than wild-type Htt, and this interaction facilitates a wide range of downstream cellular functions. Muma and coworkers prepared several deletion mutants of CaM and found that a fragment corresponding to 76-121 amino acids of CaM (CaM-peptide) is responsible for binding with mutant Htt [69]. They demonstrated that expression of CaM-peptide reduced cytotoxicity by disrupting the abnormal interaction between endogenous CaM and mutant Htt in cellular models [69, 70] and improved disease phenotypes including body weight loss and motor dysfunctions in a mouse model of HD [71]. The studies on both IC10 and CaM peptides strongly indicate that abnormal interactions of the expanded polyQ proteins is critical for polyQ disease pathogenesis, and that molecules targeting these abnormal interactions may be promising lead compounds for polyQ disease treatment.

BIP

It has been reported that expanded polyQ proteins directly induce apoptosis. Mutant Htt with expanded polyQ stretch was shown to activate p53 and increase the expression level of Bax, a proapoptotic member of the Bcl-2 family of proteins that play a key role in programmed cell death in neurons [72]. Similarly, activation of Bax and subsequent cell death has also been shown in cells expressing polyQ-expanded ataxin-3 and ataxin-7, causative proteins of SCA3 and SCA7, respectively [73, 74]. Matsuyama, Yokota and coworkers found that the proapoptotic activity of Bax is normally suppressed by Ku70, a cytoprotective protein that interacts with Bax and prevents its mitochondrial translocation, while in SCA3, mutant ataxin-3 abnormally stimulates the acetylation of Ku70, which results in dissociation of Bax from Ku70 and promotes the subsequent activation of apoptosis [75]. Importantly, expression of Ku70 effectively blocked mutant ataxin-3-induced cell death, which strongly indicates that approaches targeting the activation process of Bax could be effective for suppression of the eventual apoptosis induced by expanded polyQ proteins [75]. To develop peptide-based suppressors of Bax-induced apoptosis, they identified the Bax-binding domain of Ku70 and designed a penta-peptide, Bax-inhibiting peptide (BIP) derived from this domain [76]. BIP is particularly promising since this is cell-permeable and effectively suppresses the mitochondrial translocation of Bax and subsequent apoptotic cell death [75].

Exendin-4

Although the polyQ diseases are considered primarily as neurological disorders, patients also exhibit peripheral symptoms. In HD, it is known that patients suffer from various metabolic abnormalities including progressive weight loss, appetite dysfunction and poor glycemic control [77-80]. Similarly, mouse models of HD also exhibit these symptoms, together with impaired glucose metabolism in both brain and periphery and elevated blood glucose levels [81, 82]. This is probably due to the significant toxicity caused by high levels of mutant Htt in peripheral tissues including the pancreatic islet cells, leading to decrease in β-cell mass and impaired insulin release capacity [81, 82]. Since molecules that improve abnormal energy metabolism such as creatine have been shown to work as a neuroprotective agent and to delay the onset of motor dysfunction in a mouse model of HD [83], therapeutic approaches targeting this diabetic-like condition may be promising. Exendin-4 (Ex-4) is an agonist for glucagon-like peptide-1 receptor, and is used as a peptide drug for diabetes to improve glucose regulation [84]. Martin *et al.* tested the effects of Ex-4 on a mouse model of HD, and found that daily administration of Ex-4 by subcutaneous injection improved motor dysfunction and extended the life span of HD mice [85]. They also found that Ex-4 injection significantly promoted pancreatic β-cell growth and reduced Htt aggregates in the pancreas as well as in the brain cortex [85]. This study strongly indicates that therapeutic approaches targeting not only the central pathophysiologies but also the peripheral symptoms could be an effective strategy for treatment of the polyQ diseases.

Leuprorelin

SBMA is an adult-onset motor neuron disease, which is caused by the expansion of a polyQ stretch in the androgen receptor (AR) [86]. Although the specific pathogenic mechanisms of SBMA still remain unclear, the nuclear accumulation of abnormal AR proteins is thought to be respon-

sible for neuronal toxicity. Since testosterone binds to AR as a ligand and induces its nuclear translocation, reduction of the testosterone level would lead to a decrease in the eventual nuclear accumulation of mutant AR and to lower cytotoxicity [87, 88]. This idea is actually supported by the experimental fact that surgical castration significantly improved motor dysfunctions of a mouse model of SBMA [87, 89]. Katsuno *et al.* tested the effects of leuprorelin, a lutenizing hormone-releasing hormone (LHRH) peptide agonist that reduces testosterone release from the testis, and found that subcutaneous injection of leuprorelin reduced the nuclear accumulation of mutant AR in muscle and spinal cord, and improved the motor dysfunctions and extended the life span of a SBMA mouse model [90]. Furthermore, they conducted a series of clinical trials of leuprorelin including a randomized, placebo-controlled trial in a large cohort of 204 SBMA patients from 14 hospitals in Japan [91, 92]. Although clinical outcomes of leuprorelin administration for 48 weeks were limited to suppression of nuclear AR accumulation and decreased serum levels of testosterone with no significant improvement of motor functions, there is a possibility that leuprorelin could be effective in long-term trials in early-phase SBMA patients.

FUTURE DIRECTIONS

In this review, we introduced selected studies focusing on the development of peptide-based therapies for treatment of the polyQ diseases. Among them, the therapeutic approach focusing on aggregate formation of the expanded polyQ stretch, which targets the most upstream change occurring in the polyQ diseases, is considered to be most attractive because potential inhibitors are expected to suppress a large number of downstream functional abnormalities in a broad range of the polyQ diseases. However, efficient delivery into brains is always problematic in developing peptide-based drugs [93], as aggregation inhibitors developed by us [63] and by Chen *et al.* [64] both failed to demonstrate therapeutic effects on mouse models via their subcutaneous or intraperitoneal administration. Since both QBP1 and HQP09 have been shown to possess high potential to specifically and selectively suppress mutant polyQ-induced cytotoxicity, it is highly likely that they would be promising leads for development of polyQ disease drugs if given the ability to efficiently translocate across the blood-brain barrier (BBB). Therefore, it is quite clear that one of the future directions that we should progress toward is to re-design these potential peptide inhibitors into BBB-permeable molecules. Elucidating the structural basis as to how QBP1 and HQP09 inhibit aggregate formation of the expanded polyQ stretch would be helpful towards designing their small chemical analogues with high BBB permeability without loss of its inhibitory activity. Another direction is to develop effective delivery systems using carrier molecules which would efficiently deliver cargoes to the brain. Potential carriers include cell-penetrating peptides (CPPs, protein transduction domains/PTDs) [94-96], viral vectors [97, 98] and liposomes [99, 100], which may enable these peptide inhibitors to translocate through the BBB and to perform their therapeutic activities in specific regions of the brain. We hope that in the near future therapeutic approaches that are widely effective against the polyQ diseases are developed, and bring hope to many patients suffering from the currently untreatable polyQ diseases.

CONFLICT OF INTEREST

The authors confirm that this article content has no conflicts of interest.

ACKNOWLEDGEMENTS

We thank James R. Burke, Warren J. Strittmatter, Shinya Oishi and Nobutaka Fujii for their helpful discussions. The authors' work on the polyglutamine diseases is supported in part by Grants-in-Aid for Scientific Research on Priority Areas (Advanced Brain Science Project, and Research on Pathomechanisms of Brain Disorders to Y.N.) from the Ministry of Education, Culture, Sports, Science, and Technology, Japan; by Grants-in-Aid for Scientific Research (B) (to Y.N.) and Challenging Exploratory Research (to Y.N.) from the Japan Society for the Promotion of Science (JSPS), Japan; by a Grant-in-Aid for the Research Committee for Ataxic Diseases (to Y.N.) from the Ministry of Health, Labor and Welfare, Japan; and by a grant from Core Research for Evolutional Science and Technology (CREST) of the Japan Science and Technology Agency (to Y.N.). T.T. is grateful for the JSPS research fellowship.

ABBREVIATIONS

AR	=	Androgen receptor
Bax	=	Bcl-2 associated X protein
BBB	=	Blood-brain barrier
Bcl2	=	B-cell lymphoma 2
BIP	=	Bax-inhibiting peptide
CaM	=	Calmodulin
Ex-4	=	Exendin-4
HD	=	Huntington's disease
Htt	=	Huntingtin
$InsP_3R1$	=	Type 1 inositol 1,4,5-triphosphate receptor
K_d	=	Dissociation constant
LHRH	=	Lutenizing hormone-releasing hormone
MW	=	Molecular weight
PolyQ	=	Polyglutamine
PTD	=	Protein transduction domain
QBP1	=	PolyQ binding peptide 1
SBMA	=	Spinal and bulbar muscular atrophy
SCA	=	Spinocerebeller ataxia

REFERENCES

[1] Gusella, J.F.; MacDonald, M.E. Molecular genetics: unmasking polyglutamine triggers in neurodegenerative disease. *Nat. Rev. Neurosci.*, **2000**, *1*, 109-115.

[2] Orr, H.T.; Zoghbi, H.Y. Trinucleotide repeat disorders. *Annu. Rev. Neurosci.*, **2007**, *30*, 575-621.

[3] Nagai, Y.; Popiel, H.A. Conformational changes and aggregation of expanded polyglutamine proteins as therapeutic targets of the

polyglutamine diseases: exposed beta-sheet hypothesis. *Curr. Pharm. Des.,* **2008**, *14*, 3267-3279.

[4] The Huntington's Disease Collaborative Research Group. A novel gene containing a trinucleotide repeat that is expanded and unstable on Huntington's disease chromosomes. *Cell,* **1993**, *72*, 971-983.

[5] Doyu, M.; Sobue, G.; Mukai, E.; Kachi, T.; Yasuda, T.; Mitsuma, T.; Takahashi, A. Severity of X-linked recessive bulbospinal neuronopathy correlates with size of the tandem CAG repeat in androgen receptor gene. *Ann. Neurol.,* **1992**, *32*, 707-710.

[6] Igarashi, S.; Tanno, Y.; Onodera, O.; Yamazaki, M.; Sato, S.; Ishikawa, A.; Miyatani, N.; Nagashima, M.; Ishikawa, Y.; Sahashi, K.; *et al.* Strong correlation between the number of CAG repeats in androgen receptor genes and the clinical onset of features of spinal and bulbar muscular atrophy. *Neurology,* **1992**, *42*, 2300-2302.

[7] Mangiarini, L.; Sathasivam, K.; Seller, M.; Cozens, B.; Harper, A.; Hetherington, C.; Lawton, M.; Trottier, Y.; Lehrach, H.; Davies, S. W.; Bates, G. P. Exon 1 of the HD gene with an expanded CAG repeat is sufficient to cause a progressive neurological phenotype in transgenic mice. *Cell,* **1996**, *87*, 493-506.

[8] Ikeda, H.; Yamaguchi, M.; Sugai, S.; Aze, Y.; Narumiya, S.; Kakizuka, A. Expanded polyglutamine in the Machado-Joseph disease protein induces cell death *in vitro* and *in vivo*. *Nat. Genet.,* **1996**, *13*, 196-202.

[9] Burright, E.N.; Clark, H.B.; Servadio, A.; Matilla, T.; Feddersen, R.M.; Yunis, W.S.; Duvick, L.A.; Zoghbi, H.Y.; Orr, H.T. SCA1 transgenic mice: a model for neurodegeneration caused by an expanded CAG trinucleotide repeat. *Cell,* **1995**, *82*, 937-948.

[10] Warrick, J.M.; Paulson, H.L.; Gray-Board, G.L.; Bui, Q.T.; Fischbeck, K.H.; Pittman, R.N.; Bonini, N.M. Expanded polyglutamine protein forms nuclear inclusions and causes neural degeneration in Drosophila. *Cell,* **1998**, *93*, 939-949.

[11] Faber, P.W.; Alter, J.R.; MacDonald, M.E.; Hart, A.C. Polyglutamine-mediated dysfunction and apoptotic death of a Caenorhabditis elegans sensory neuron. *Proc. Natl. Acad. Sci. USA,* **1999**, *96*, 179-184.

[12] Ross, C.A. Polyglutamine pathogenesis: emergence of unifying mechanisms for Huntington's disease and related disorders. *Neuron,* **2002**, *35*, 819-822.

[13] Shao, J.; Diamond, M.I. Polyglutamine diseases: emerging concepts in pathogenesis and therapy. *Hum. Mol. Genet.,* **2007**, *16 Spec No. 2*, R115-R123.

[14] Scherzinger, E.; Lurz, R.; Turmaine, M.; Mangiarini, L.; Hollenbach, B.; Hasenbank, R.; Bates, G. P.; Davies, S.W.; Lehrach, H.; Wanker, E.E. Huntingtin-encoded polyglutamine expansions form amyloid-like protein aggregates *in vitro* and *in vivo*. *Cell,* **1997**, *90*, 549-558.

[15] Scherzinger, E.; Sittler, A.; Schweiger, K.; Heiser, V.; Lurz, R.; Hasenbank, R.; Bates, G.P.; Lehrach, H.; Wanker, E.E. Self-assembly of polyglutamine-containing huntingtin fragments into amyloid-like fibrils: implications for Huntington's disease pathology. *Proc. Natl. Acad. Sci. USA,* **1999**, *96*, 4604-4609.

[16] Chen, S.; Berthelier, V.; Yang, W.; Wetzel, R. Polyglutamine aggregation behavior *in vitro* supports a recruitment mechanism of cytotoxicity. *J. Mol. Biol.,* **2001**, *311*, 173-182.

[17] Yang, W.; Dunlap, J.R.; Andrews, R.B.; Wetzel, R. Aggregated polyglutamine peptides delivered to nuclei are toxic to mammalian cells. *Hum. Mol. Genet.,* **2002**, *11*, 2905-2917.

[18] Wetzel, R. Physical chemistry of polyglutamine: intriguing tales of a monotonous sequence. *J. Mol. Biol.,* **2012**, *421*, 466-490.

[19] Kuemmerle, S.; Gutekunst, C.A.; Klein, A.M.; Li, X.J.; Li, S.H.; Beal, M.F.; Hersch, S.M.; Ferrante, R.J. Huntington aggregates may not predict neuronal death in Huntington's disease. *Ann. Neurol.,* **1999**, *46*, 842-849.

[20] Klement, I.A.; Skinner, P.J.; Kaytor, M.D.; Yi, H.; Hersch, S.M.; Clark, H.B.; Zoghbi, H.Y.; Orr, H.T. Ataxin-1 nuclear localization and aggregation: role in polyglutamine-induced disease in SCA1 transgenic mice. *Cell,* **1998**, *95*, 41-53.

[21] Saudou, F.; Finkbeiner, S.; Devys, D.; Greenberg, M.E. Huntingtin acts in the nucleus to induce apoptosis but death does not correlate with the formation of intranuclear inclusions. *Cell,* **1998**, *95*, 55-66.

[22] Arrasate, M.; Mitra, S.; Schweitzer, E.S.; Segal, M.R.; Finkbeiner, S. Inclusion body formation reduces levels of mutant huntingtin and the risk of neuronal death. *Nature,* **2004**, *431*, 805-810.

[23] Nagai, Y.; Inui, T.; Popiel, H.A.; Fujikake, N.; Hasegawa, K.; Urade, Y.; Goto, Y.; Naiki, H.; Toda, T. A toxic monomeric conformer of the polyglutamine protein. *Nat. Struct. Mol. Biol.,* **2007**, *14*, 332-340.

[24] Cummings, C.J.; Mancini, M.A.; Antalffy, B.; DeFranco, D.B.; Orr, H.T.; Zoghbi, H.Y. Chaperone suppression of aggregation and altered subcellular proteasome localization imply protein misfolding in SCA1. *Nat. Genet.,* **1998**, *19*, 148-154.

[25] Warrick, J.M.; Chan, H.Y.; Gray-Board, G.L.; Chai, Y.; Paulson, H.L.; Bonini, N.M. Suppression of polyglutamine-mediated neurodegeneration in Drosophila by the molecular chaperone HSP70. *Nat. Genet.,* **1999**, *23*, 425-428.

[26] Sittler, A.; Lurz, R.; Lueder, G.; Priller, J.; Lehrach, H.; Hayer-Hartl, M.K.; Hartl, F.U.; Wanker, E.E. Geldanamycin activates a heat shock response and inhibits huntingtin aggregation in a cell culture model of Huntington's disease. *Hum. Mol. Genet.,* **2001**, *10*, 1307-1315.

[27] Katsuno, M.; Sang, C.; Adachi, H.; Minamiyama, M.; Waza, M.; Tanaka, F.; Doyu, M.; Sobue, G. Pharmacological induction of heat-shock proteins alleviates polyglutamine-mediated motor neuron disease. *Proc. Natl. Acad. Sci. USA,* **2005**, *102*, 16801-16806.

[28] Fujikake, N.; Nagai, Y.; Popiel, H.A.; Okamoto, Y.; Yamaguchi, M.; Toda, T. Heat shock transcription factor 1-activating compounds suppress polyglutamine-induced neurodegeneration through induction of multiple molecular chaperones. *J. Biol. Chem.,* **2008**, *283*, 26188-26197.

[29] Lecerf, J.M.; Shirley, T.L.; Zhu, Q.; Kazantsev, A.; Amersdorfer, P.; Housman, D.E.; Messer, A.; Huston, J.S. Human single-chain Fv intrabodies counteract *in situ* huntingtin aggregation in cellular models of Huntington's disease. *Proc. Natl. Acad. Sci. USA,* **2001**, *98*, 4764-4769.

[30] Colby, D.W.; Chu, Y.; Cassady, J.P.; Duennwald, M.; Zazulak, H.; Webster, J.M.; Messer, A.; Lindquist, S.; Ingram, V.M.; Wittrup, K.D. Potent inhibition of huntingtin aggregation and cytotoxicity by a disulfide bond-free single-domain intracellular antibody. *Proc. Natl. Acad. Sci. USA,* **2004**, *101*, 17616-17621.

[31] Wolfgang, W.J.; Miller, T.W.; Webster, J.M.; Huston, J.S.; Thompson, L.M.; Marsh, J.L.; Messer, A. *Proc. Natl. Acad. Sci. USA,* **2005**, *102*, 11563-11568.

[32] Nagai, Y.; Fujikake, N.; Popiel, H.A.; Wada, K. Induction of molecular chaperones as a therapeutic strategy for the polyglutamine diseases. *Curr. Pharm. Biotechnol.,* **2010**, *11*, 188-197.

[33] Butler, D.C.; McLear, J.A.; Messer, A. Engineered antibody therapies to counteract mutant huntingtin and related toxic intracellular proteins. *Prog. Neurobiol.,* **2012**, *97*, 190-204.

[34] Heiser, V.; Scherzinger, E.; Boeddrich, A.; Nordhoff, E.; Lurz, R.; Schugardt, N.; Lehrach, H.; Wanker, E.E. Inhibition of huntingtin fibrillogenesis by specific antibodies and small molecules: implications for Huntington's disease therapy. *Proc. Natl. Acad. Sci. USA,* **2000**, *97*, 6739-6744.

[35] Heiser, V.; Engemann, S.; Brocker, W.; Dunkel, I.; Boeddrich, A.; Waelter, S.; Nordhoff, E.; Lurz, R.; Schugardt, N.; Rautenberg, S.; Herhaus, C.; Barnickel, G.; Bottcher, H.; Lehrach, H.; Wanker, E.E. Identification of benzothiazoles as potential polyglutamine aggregation inhibitors of Huntington's disease by using an automated filter retardation assay. *Proc. Natl. Acad. Sci. USA,* **2002**, *99 Suppl 4*, 16400-16406.

[36] Tanaka, M.; Machida, Y.; Niu, S.; Ikeda, T.; Jana, N.R.; Doi, H.; Kurosawa, M.; Nekooki, M.; Nukina, N. Trehalose alleviates polyglutamine-mediated pathology in a mouse model of Huntington disease. *Nat. Med.,* **2004**, *10*, 148-154.

[37] Wang, J.; Gines, S.; MacDonald, M.E.; Gusella, J.F. Reversal of a full-length mutant huntingtin neuronal cell phenotype by chemical inhibitors of polyglutamine-mediated aggregation. *BMC. Neurosci.,* **2005**, *6*, 1.

[38] Ehrnhoefer, D.E.; Duennwald, M.; Markovic, P.; Wacker, J.L.; Engemann, S.; Roark, M.; Legleiter, J.; Marsh, J.L.; Thompson, L.M.; Lindquist, S.; Muchowski, P.J.; Wanker, E.E. Green tea (-)-epigallocatechin-gallate modulates early events in huntingtin misfolding and reduces toxicity in Huntington's disease models. *Hum. Mol. Genet.,* **2006**, *15*, 2743-2751.

[39] Nagai, Y.; Tucker, T.; Ren, H.; Kenan, D.J.; Henderson, B.S.; Keene, J.D.; Strittmatter, W.J.; Burke, J.R. Inhibition of polyglutamine protein aggregation and cell death by novel peptides identified by phage display screening. *J. Biol. Chem.,* **2000**, *275*, 10437-10442.

[40] Kazantsev, A.; Walker, H.A.; Slepko, N.; Bear, J.E.; Preisinger, E.; Steffan, J.S.; Zhu, Y.Z.; Gertler, F.B.; Housman, D.E.; Marsh, J.L.; Thompson, L.M. A bivalent Huntingtin binding peptide suppresses polyglutamine aggregation and pathogenesis in Drosophila. *Nat. Genet.,* **2002**, *30*, 367-376.

[41] Popiel, H.A.; Nagai, Y.; Onodera, O.; Inui, T.; Fujikake, N.; Urade, Y.; Strittmatter, W.J.; Burke, J.R.; Ichikawa, A.; Toda, T. Disruption of the toxic conformation of the expanded polyglutamine stretch leads to suppression of aggregate formation and cytotoxicity. *Biochem. Biophys. Res. Commun.,* **2004**, *317*, 1200-1206.

[42] Bauer, P.O.; Goswami, A.; Wong, H.K.; Okuno, M.; Kurosawa, M.; Yamada, M.; Miyazaki, H.; Matsumoto, G.; Kino, Y.; Nagai, Y.; Nukina, N. Harnessing chaperone-mediated autophagy for the selective degradation of mutant huntingtin protein. *Nat. Biotechnol.,* **2010**, *28*, 256-263.

[43] Shoji-Kawata, S.; Sumpter, R.; Leveno, M.; Campbell, G.R.; Zou, Z.; Kinch, L.; Wilkins, A.D.; Sun, Q.; Pallauf, K.; MacDuff, D.; Huerta, C.; Virgin, H.W.; Helms, J.B.; Eerland, R.; Tooze, S.A.; Xavier, R.; Lenschow, D.J.; Yamamoto, A.; King, D.; Lichtarge, O.; Grishin, N.V.; Spector, S.A.; Kaloyanova, D.V.; Levine, B. Identification of a candidate therapeutic autophagy-inducing peptide. *Nature,* **2013**, *494*, 201-206.

[44] Steffan, J.S.; Kazantsev, A.; Spasic-Boskovic, O.; Greenwald, M.; Zhu, Y.Z.; Gohler, H.; Wanker, E.E.; Bates, G.P.; Housman, D.E.; Thompson, L.M. The Huntington's disease protein interacts with p53 and CREB-binding protein and represses transcription. *Proc. Natl. Acad. Sci. USA,* **2000**, *97*, 6763-6768.

[45] Bence, N.F.; Sampat, R.M.; Kopito, R.R. Impairment of the ubiquitin-proteasome system by protein aggregation. *Science,* **2001**, *292*, 1552-1555.

[46] Romero, E.; Cha, G.H.; Verstreken, P.; Ly, C.V.; Hughes, R.E.; Bellen, H.J.; Botas, J. Suppression of neurodegeneration and increased neurotransmission caused by expanded full-length huntingtin accumulating in the cytoplasm. *Neuron,* **2008**, *57*, 27-40.

[47] Gunawardena, S.; Her, L.S.; Brusch, R.G.; Laymon, R.A.; Niesman, I.R.; Gordesky-Gold, B.; Sintasath, L.; Bonini, N.M.; Goldstein, L.S. Disruption of axonal transport by loss of huntingtin or expression of pathogenic polyQ proteins in Drosophila. *Neuron,* **2003**, *40*, 25-40.

[48] Tang, T.S.; Tu, H.; Chan, E.Y.; Maximov, A.; Wang, Z.; Wellington, C.L.; Hayden, M.R.; Bezprozvanny, I. Huntingtin and huntingtin-associated protein 1 influence neuronal calcium signaling mediated by inositol-(1,4,5) triphosphate receptor type 1. *Neuron,* **2003**, *39*, 227-239.

[49] Tobin, A.J.; Signer, E.R. Huntington's disease: the challenge for cell biologists. *Trends Cell Biol.,* **2000**, *10*, 531-536.

[50] Harjes, P.; Wanker, E.E. The hunt for huntingtin function: interaction partners tell many different stories. *Trends Biochem. Sci.,* **2003**, *28*, 425-433.

[51] Trottier, Y.; Lutz, Y.; Stevanin, G.; Imbert, G.; Devys, D.; Cancel, G.; Saudou, F.; Weber, C.; David, G.; Tora, L.; Agid, Y.; Brice, A.; Mandel, J. Polyglutamine expansion as a pathological epitope in Huntington's disease and four dominant cerebellar ataxias. *Nature,* **1995**, *378*, 403-406.

[52] Bennett, M.J.; Huey-Tubman, K.E.; Herr, A.B.; West, A.P., Jr.; Ross, S.A.; Bjorkman, P.J. A linear lattice model for polyglutamine in CAG-expansion diseases. *Proc. Natl. Acad. Sci. USA,* **2002**, *99*, 11634-11639.

[53] Miller, J.; Arrasate, M.; Brooks, E.; Libeu, C.P.; Legleiter, J.; Hatters, D.; Curtis, J.; Cheung, K.; Krishnan, P.; Mitra, S.; Widjaja, K.; Shaby, B.A.; Lotz, G.P.; Newhouse, Y.; Mitchell, E.J.; Osmand, A.; Gray, M.; Thulasiramin, V.; Saudou, F.; Segal, M.; Yang, X.W.; Masliah, E.; Thompson, L.M.; Muchowski, P.J.; Weisgraber, K.H.; Finkbeiner, S. Identifying polyglutamine protein species in situ that best predict neurodegeneration. *Nat. Chem. Biol.,* **2011**, *7*, 925-934.

[54] Okamoto, Y.; Nagai, Y.; Fujikake, N.; Popiel, H.A.; Yoshioka, T.; Toda, T.; Inui, T. Surface plasmon resonance characterization of specific binding of polyglutamine aggregation inhibitors to the expanded polyglutamine stretch. *Biochem. Biophys. Res. Commun.,* **2009**, *378*, 634-639.

[55] Ren, H.; Nagai, Y.; Tucker, T.; Strittmatter, W.J.; Burke, J.R. Amino acid sequence requirements of peptides that inhibit polyglutamine-protein aggregation and cell death. *Biochem. Biophys. Res. Commun.,* **2001**, *288*, 703-710.

[56] Tomita, K.; Popiel, H.A.; Nagai, Y.; Toda, T.; Yoshimitsu, Y.; Ohno, H.; Oishi, S.; Fujii, N. Structure-activity relationship study on polyglutamine binding peptide QBP1. *Bioorg. Med. Chem.,* **2009**, *17*, 1259-1263.

[57] Hamuro, L.; Zhang, G.; Tucker, T.J.; Self, C.; Strittmatter, W.J.; Burke, J.R. Optimization of a polyglutamine aggregation inhibitor peptide (QBP1) using a thioflavin T fluorescence assay. *Assay Drug Dev. Technol.,* **2007**, *5*, 629-636.

[58] Takahashi, Y.; Okamoto, Y.; Popiel, H.A.; Fujikake, N.; Toda, T.; Kinjo, M.; Nagai, Y. Detection of polyglutamine protein oligomers in cells by fluorescence correlation spectroscopy. *J. Biol. Chem.,* **2007**, *282*, 24039-24048.

[59] Takahashi, T.; Kikuchi, S.; Katada, S.; Nagai, Y.; Nishizawa, M.; Onodera, O. Soluble polyglutamine oligomers formed prior to inclusion body formation are cytotoxic. *Hum. Mol. Genet.,* **2008**, *17*, 345-356.

[60] Nagai, Y.; Fujikake, N.; Ohno, K.; Higashiyama, H.; Popiel, H.A.; Rahadian, J.; Yamaguchi, M.; Strittmatter, W.J.; Burke, J.R.; Toda, T. Prevention of polyglutamine oligomerization and neurodegeneration by the peptide inhibitor QBP1 in Drosophila. *Hum. Mol. Genet.,* **2003**, *12*, 1253-1259.

[61] Futaki, S.; Hirose, H.; Nakase, I. Arginine-rich peptides: methods of translocation through biological membranes. *Curr. Pharm. Des.,* **2012**, *19*, 2863-2868.

[62] Popiel, H.A.; Nagai, Y.; Fujikake, N.; Toda, T. Protein transduction domain-mediated delivery of QBP1 suppresses polyglutamine-induced neurodegeneration in vivo. *Mol. Ther.,* **2007**, *15*, 303-309.

[63] Popiel, H.A.; Nagai, Y.; Fujikake, N.; Toda, T. Delivery of the aggregate inhibitor peptide QBP1 into the mouse brain using PTDs and its therapeutic effect on polyglutamine disease mice. *Neurosci. Lett.,* **2009**, *449*, 87-92.

[64] Chen, X.; Wu, J.; Luo, Y.; Liang, X.; Supnet, C.; Kim, M.W.; Lotz, G.P.; Yang, G.; Muchowski, P.J.; Kodadek, T.; Bezprozvanny, I. Expanded polyglutamine-binding peptoid as a novel therapeutic agent for treatment of Huntington's disease. *Chem. Biol.,* **2011**, *18*, 1113-1125.

[65] Simon, R.J.; Kania, R.S.; Zuckermann, R.N.; Huebner, V.D.; Jewell, D.A.; Banville, S.; Ng, S.; Wang, L.; Rosenberg, S.; Marlowe, C.K.; Spellmeyer, D.C.; Tan, R.; Frankel, A.D.; Santi, D.V.; Cohen, F.E.; Bartlett, P.A. Peptoids: a modular approach to drug discovery. *Proc. Natl. Acad. Sci. USA,* **1992**, *89*, 9367-9371.

[66] Zuckermann, R.N.; Kodadek, T. Peptoids as potential therapeutics. *Curr. Opin. Mol. Ther.,* **2009**, *11*, 299-307.

[67] Tang, T.S.; Tu, H.; Orban, P.C.; Chan, E.Y.; Hayden, M.R.; Bezprozvanny, I. HAP1 facilitates effects of mutant huntingtin on inositol 1,4,5-trisphosphate-induced Ca release in primary culture of striatal medium spiny neurons. *Eur. J. Neurosci.,* **2004**, *20*, 1779-1787.

[68] Tang, T.S.; Guo, C.; Wang, H.; Chen, X.; Bezprozvanny, I. Neuroprotective effects of inositol 1,4,5-trisphosphate receptor C-terminal fragment in a Huntington's disease mouse model. *J. Neurosci.,* **2009**, *29*, 1257-1266.

[69] Dudek, N.L.; Dai, Y.; Muma, N.A. Protective effects of interrupting the binding of calmodulin to mutant huntingtin. *J. Neuropathol. Exp. Neurol.,* **2008**, *67*, 355-365.

[70] Dudek, N.L.; Dai, Y.; Muma, N.A. Neuroprotective effects of calmodulin peptide 76-121aa: disruption of calmodulin binding to mutant huntingtin. *Brain Pathol.,* **2010**, *20*, 176-189.

[71] Dai, Y.; Dudek, N.L.; Li, Q.; Fowler, S.C.; Muma, N.A. Striatal expression of a calmodulin fragment improved motor function, weight loss, and neuropathology in the R6/2 mouse model of Huntington's disease. *J. Neurosci.,* **2009**, *29*, 11550-11559.

[72] Bae, B.I.; Xu, H.; Igarashi, S.; Fujimuro, M.; Agrawal, N.; Taya, Y.; Hayward, S.D.; Moran, T.H.; Montell, C.; Ross, C.A.; Snyder, S.H.; Sawa, A. p53 mediates cellular dysfunction and behavioral abnormalities in Huntington's disease. *Neuron,* **2005**, *47*, 29-41.

[73] Chou, A.H.; Yeh, T.H.; Kuo, Y.L.; Kao, Y.C.; Jou, M.J.; Hsu, C.Y.; Tsai, S.R.; Kakizuka, A.; Wang, H.L. Polyglutamine-expanded ataxin-3 activates mitochondrial apoptotic pathway by upregulating Bax and downregulating Bcl-xL. *Neurobiol. Dis.,* **2006**, *21*, 333-345.

[74] Wang, H.L.; Yeh, T.H.; Chou, A.H.; Kuo, Y.L.; Luo, L.J.; He, C.Y.; Huang, P.C.; Li, A.H. Polyglutamine-expanded ataxin-7 activates mitochondrial apoptotic pathway of cerebellar neurons by

upregulating Bax and downregulating Bcl-x(L). *Cell. Signal.,* **2006**, *18*, 541-552.

[75] Li, Y.; Yokota, T.; Gama, V.; Yoshida, T.; Gomez, J.A.; Ishikawa, K.; Sasaguri, H.; Cohen, H.Y.; Sinclair, D.A.; Mizusawa, H.; Matsuyama, S. Bax-inhibiting peptide protects cells from polyglutamine toxicity caused by Ku70 acetylation. *Cell Death Differ.,* **2007**, *14*, 2058-2067.

[76] Yoshida, T.; Tomioka, I.; Nagahara, T.; Holyst, T.; Sawada, M.; Hayes, P.; Gama, V.; Okuno, M.; Chen, Y.; Abe, Y.; Kanouchi, T.; Sasada, H.; Wang, D.; Yokota, T.; Sato, E.; Matsuyama, S. Bax-inhibiting peptide derived from mouse and rat Ku70. *Biochem. Biophys. Res. Commun.,* **2004**, *321*, 961-966.

[77] Aziz, N.A.; Swaab, D.F.; Pijl, H.; Roos, R.A. Hypothalamic dysfunction and neuroendocrine and metabolic alterations in Huntington's disease: clinical consequences and therapeutic implications. *Rev. Neurosci.,* **2007**, *18*, 223-251.

[78] Powers, W.J.; Videen, T.O.; Markham, J.; McGee-Minnich, L.; Antenor-Dorsey, J.V.; Hershey, T.; Perlmutter, J.S. Selective defect of in vivo glycolysis in early Huntington's disease striatum. *Proc. Natl. Acad. Sci. USA,* **2007**, *104*, 2945-2949.

[79] Gaba, A.M.; Zhang, K.; Marder, K.; Moskowitz, C.B.; Werner, P.; Boozer, C.N. Energy balance in early-stage Huntington disease. *Am. J. Clin. Nutr.,* **2005**, *81*, 1335-1341.

[80] Lodi, R.; Schapira, A.H.; Manners, D.; Styles, P.; Wood, N.W.; Taylor, D.J.; Warner, T.T. Abnormal in vivo skeletal muscle energy metabolism in Huntington's disease and dentatorubropallidoluysian atrophy. *Ann. Neurol.,* **2000**, *48*, 72-76.

[81] Hurlbert, M.S.; Zhou, W.; Wasmeier, C.; Kaddis, F.G.; Hutton, J.C.; Freed, C.R. Mice transgenic for an expanded CAG repeat in the Huntington's disease gene develop diabetes. *Diabetes,* **1999**, *48*, 649-651.

[82] Bjorkqvist, M.; Fex, M.; Renstrom, E.; Wierup, N.; Petersen, A.; Gil, J.; Bacos, K.; Popovic, N.; Li, J.Y.; Sundler, F.; Brundin, P.; Mulder, H. The R6/2 transgenic mouse model of Huntington's disease develops diabetes due to deficient beta-cell mass and exocytosis. *Hum. Mol. Genet.,* **2005**, *14*, 565-574.

[83] Ferrante, R.J.; Andreassen, O.A.; Jenkins, B.G.; Dedeoglu, A.; Kuemmerle, S.; Kubilus, J.K.; Kaddurah-Daouk, R.; Hersch, S.M.; Beal, M.F. Neuroprotective effects of creatine in a transgenic mouse model of Huntington's disease. *J. Neurosci.,* **2000**, *20*, 4389-4397.

[84] Greig, N.H.; Holloway, H.W.; De Ore, K.A.; Jani, D.; Wang, Y.; Zhou, J.; Garant, M. J.; Egan, J.M. Once daily injection of exendin-4 to diabetic mice achieves long-term beneficial effects on blood glucose concentrations. *Diabetologia,* **1999**, *42*, 45-50.

[85] Martin, B.; Golden, E.; Carlson, O.D.; Pistell, P.; Zhou, J.; Kim, W.; Frank, B.P.; Thomas, S.; Chadwick, W.A.; Greig, N.H.; Bates, G.P.; Sathasivam, K.; Bernier, M.; Maudsley, S.; Mattson, M.P.; Egan, J.M. Exendin-4 improves glycemic control, ameliorates brain and pancreatic pathologies, and extends survival in a mouse model of Huntington's disease. *Diabetes,* **2009**, *58*, 318-328.

[86] Katsuno, M.; Tanaka, F.; Adachi, H.; Banno, H.; Suzuki, K.; Watanabe, H.; Sobue, G. Pathogenesis and therapy of spinal and bulbar muscular atrophy (SBMA). *Prog. Neurobiol.,* **2012**, *99*, 246-256.

[87] Katsuno, M.; Adachi, H.; Kume, A.; Li, M.; Nakagomi, Y.; Niwa, H.; Sang, C.; Kobayashi, Y.; Doyu, M.; Sobue, G. Testosterone reduction prevents phenotypic expression in a transgenic mouse model of spinal and bulbar muscular atrophy. *Neuron,* **2002**, *35*, 843-854.

[88] Takeyama, K.; Ito, S.; Yamamoto, A.; Tanimoto, H.; Furutani, T.; Kanuka, H.; Miura, M.; Tabata, T.; Kato, S. Androgen-dependent neurodegeneration by polyglutamine-expanded human androgen receptor in Drosophila. *Neuron,* **2002**, *35*, 855-864.

[89] Chevalier-Larsen, E.S.; O'Brien, C.J.; Wang, H.; Jenkins, S.C.; Holder, L.; Lieberman, A.P.; Merry, D.E. Castration restores function and neurofilament alterations of aged symptomatic males in a transgenic mouse model of spinal and bulbar muscular atrophy. *J. Neurosci.,* **2004**, *24*, 4778-4786.

[90] Katsuno, M.; Adachi, H.; Doyu, M.; Minamiyama, M.; Sang, C.; Kobayashi, Y.; Inukai, A.; Sobue, G. Leuprorelin rescues polyglutamine-dependent phenotypes in a transgenic mouse model of spinal and bulbar muscular atrophy. *Nat. Med.,* **2003**, *9*, 768-773.

[91] Banno, H.; Katsuno, M.; Suzuki, K.; Takeuchi, Y.; Kawashima, M.; Suga, N.; Takamori, M.; Ito, M.; Nakamura, T.; Matsuo, K.; Yamada, S.; Oki, Y.; Adachi, H.; Minamiyama, M.; Waza, M.; Atsuta, N.; Watanabe, H.; Fujimoto, Y.; Nakashima, T.; Tanaka, F.; Doyu, M.; Sobue, G. Phase 2 trial of leuprorelin in patients with spinal and bulbar muscular atrophy. *Ann. Neurol.,* **2009**, *65*, 140-150.

[92] Katsuno, M.; Banno, H.; Suzuki, K.; Takeuchi, Y.; Kawashima, M.; Yabe, I.; Sasaki, H.; Aoki, M.; Morita, M.; Nakano, I.; Kanai, K.; Ito, S.; Ishikawa, K.; Mizusawa, H.; Yamamoto, T.; Tsuji, S.; Hasegawa, K.; Shimohata, T.; Nishizawa, M.; Miyajima, H.; Kanda, F.; Watanabe, Y.; Nakashima, K.; Tsujino, A.; Yamashita, T.; Uchino, M.; Fujimoto, Y.; Tanaka, F.; Sobue, G. Efficacy and safety of leuprorelin in patients with spinal and bulbar muscular atrophy (JASMITT study): a multicentre, randomised, double-blind, placebo-controlled trial. *Lancet Neurol.,* **2010**, *9*, 875-884.

[93] Craik, D.J.; Fairlie, D.P.; Liras, S.; Price, D. The Future of Peptide-based Drugs. *Chem. Biol. Drug Des.,* **2013**, *81*, 136-147.

[94] Asoh, S.; Ohta, S. PTD-mediated delivery of anti-cell death proteins/peptides and therapeutic enzymes. *Adv. Drug Deliv. Rev.,* **2008**, *60*, 499-516.

[95] Blumling Iii, J.P.; Silva, G.A. Targeting the brain: advances in drug delivery. *Curr. Pharm. Biotechnol.,* **2012**, *13*, 2417-2426.

[96] Malakoutikhah, M.; Teixidó, M.; Giralt, E. Shuttle-mediated drug delivery to the brain. *Angew. Chem. Int. Ed.,* **2011**, *50*, 7998-8014.

[97] Salegio, E.A.; Samaranch, L.; Kells, A.P.; Forsayeth, J.; Bankiewicz, K. Guided delivery of adeno-associated viral vectors into the primate brain. *Adv. Drug Deliv. Rev.,* **2012**, *64*, 598-604.

[98] Hester, M.E.; Foust, K.D.; Kaspar, R.W.; Kaspar, B.K. AAV as a gene transfer vector for the treatment of neurological disorders: novel treatment thoughts for ALS. *Curr. Gene Ther.,* **2009**, *9*, 428-433.

[99] Garbayo, E.; Ansorena, E.; Blanco-Prieto, M.J. Brain drug delivery systems for neurodegenerative disorders. *Curr. Pharm. Biotechnol.,* **2012**, *13*, 2388-2402.

[100] Micheli, M.R.; Bova, R.; Magini, A.; Polidoro, M.; Emiliani, C. Lipid-based nanocarriers for CNS-targeted drug delivery. *Recent Pat. CNS Drug Discov.,* **2012**, *7*, 71-86.

Received: ????????????????? **Revised:** ????????????????? **Accepted:** ?????????????????

Human Molecular Genetics, 2014, Vol. 23, No. 13 **3467–3480**
doi:10.1093/hmg/ddu055
Advance Access published on February 4, 2014

Identification of *ter94*, *Drosophila VCP*, as a strong modulator of motor neuron degeneration induced by knockdown of *Caz*, *Drosophila FUS*

Yumiko Azuma[1], Takahiko Tokuda[1,2,†,*], Mai Shimamura[3,4], Akane Kyotani[3,4], Hiroshi Sasayama[1], Tomokatsu Yoshida[1], Ikuko Mizuta[1], Toshiki Mizuno[1], Masanori Nakagawa[1], Nobuhiro Fujikake[5], Morio Ueyama[5], Yoshitaka Nagai[5] and Masamitsu Yamaguchi[3,4,†]

[1]Department of Neurology and [2]Department of Molecular Pathobiology of Brain Diseases, Graduate School of Medical Science, Kyoto Prefectural University of Medicine, 465 Kajii-cho, Kamigyo-ku, Kyoto 602-8566, Japan, [3]Department of Applied Biology and [4]Insect Biomedical Research Center, Kyoto Institute of Technology, Hashikami-cho, Matsugasaki, Sakyo-ku, Kyoto 606-8585, Japan and [5]Department of Degenerative Neurological Diseases, National Institute of Neuroscience, National Center of Neurology and Psychiatry, 4-1-1 Ogawa-Higashi, Kodaira, Tokyo 187-8502, Japan

Received October 3, 2013; Revised and Accepted January 31, 2014

In humans, mutations in the *fused in sarcoma* (*FUS*) gene have been identified in sporadic and familial forms of amyotrophic lateral sclerosis (ALS). *Cabeza* (*Caz*) is the *Drosophila* ortholog of human *FUS*. Previously, we established *Drosophila* models of ALS harboring *Caz*-knockdown. These flies develop locomotive deficits and anatomical defects in motoneurons (MNs) at neuromuscular junctions; these phenotypes indicate that loss of physiological FUS functions in the nucleus can cause MN degeneration similar to that seen in FUS-related ALS. Here, we aimed to explore molecules that affect these ALS-like phenotypes of our *Drosophila* models with eye-specific and neuron-specific *Caz*-knockdown. We examined several previously reported ALS-related genes and found genetic links between *Caz* and *ter94*, the *Drosophila* ortholog of human *Valosin-containing protein* (*VCP*). Genetic crossing the strongest loss-of-function allele of *ter94* with *Caz*-knockdown strongly enhanced the rough-eye phenotype and the MN-degeneration phenotype caused by *Caz*-knockdown. Conversely, the overexpression of wild-type *ter94* in the background of *Caz*-knockdown remarkably suppressed those phenotypes. Our data demonstrated that expression levels of *Drosophila* VCP ortholog dramatically modified the phenotypes caused by *Caz*-knockdown in either direction, exacerbation or remission. Our results indicate that therapeutic agents that up-regulate the function of human VCP could modify the pathogenic processes that lead to the degeneration of MNs in ALS.

INTRODUCTION

Amyotrophic lateral sclerosis (ALS) is a devastating neurodegenerative disease that is characterized by degeneration of motoneurons (MNs); this degeneration leads to progressive muscle weakness and eventually fatal paralysis typically within 1–5 years after disease onset (1). Frontotemporal lobar degeneration (FTLD) is a dementia syndrome with clinically diverse phenotypes that include behavioral changes, semantic dementia and progressive non-fluent aphasia (2). It is well established that ALS and FTLD form a clinical disease continuum (3,4). Up to 15% of ALS patients meet the clinical criteria of FTLD and 30–50% has subtle cognitive deficits (5); likewise, up to 15% of FTLD patients meet the clinical criteria for ALS and up to one-third have at least minor MN dysfunction (5).

* To whom correspondence should be addressed at: Department of Molecular Pathobiology of Brain Diseases, Graduate School of Medical Science, Kyoto Prefectural University of Medicine, 465 Kajii-cho, Kamigyo-ku, Kyoto 602-8566, Japan. Tel: +81 752515793; Fax: +81 752118645; Email: ttokuda@koto.kpu-m.ac.jp
†Co-corresponding authors.

© *The Author 2014. Published by Oxford University Press. All rights reserved.*
For Permissions, please email: journals.permissions@oup.com

Downloaded from http://hmg.oxfordjournals.org/ at NCNP on July 2, 2014

A substantial number of proteins linked to ALS are directly or indirectly involved in RNA processing (6). Mutations in genes encoding two such RNA-binding proteins—transactive response DNA binding protein 43 kDa (TDP-43, gene *TARDBP*) and fused in sarcoma (FUS, gene *FUS*)—have been identified as major genetic causes in both familial and sporadic ALS (2,7–15). TDP-43 and FUS are RNA-binding proteins implicated in multiple aspects of RNA metabolism including transcriptional regulation, mRNA splicing and shuttling of mRNAs between the nucleus and the cytoplasm (16,17).

There is a single *Drosophila* ortholog each for human FUS and TDP-43 named Cabeza (Caz) and TBPH, respectively. Reportedly, *Drosophila* lacking TBPH presented deficient locomotive behaviors, reduced life span and anatomical defects at neuromuscular junctions (NMJs); these phenotypes indicate that a loss of TDP-43 nuclear functions could be a causative factor for the neurodegeneration observed in patients with ALS/FTLD (18). Recently, we reported a fly model of ALS based on neuron-specific Caz-knockdown, which developed locomotive deficits and anatomical defects in MNs at NMJs; these findings demonstrate that loss of physiological functions of FUS in the nucleus could cause the neurodegeneration in FUS-related ALS/FTLD (19). There is substantial evidence that depletion of FUS in zebrafish or in *Drosophila* also causes MN degeneration that can be rescued by the respective wild-type but not mutant *FUS* (20,21). These findings suggest that FUS is important for the survival of MNs and that a "loss-of-function" mechanism could be the fundamental pathogenic mechanism causing FUS-related ALS/FTLD.

Using our established fly model of FUS-ALS induced by *Caz*-knockdown, we aimed to explore molecules that affect phenotypes presented by the model. Specifically, we intended to elucidate the molecular mechanisms leading to neuronal dysfunction in FUS-related ALS/FTLD in order to facilitate the development of disease-modifying therapies, which are eagerly desired for the treatment of those relentless neurodegenerative diseases. Initially, we focused on determining whether or not several ALS-related genes affect the phenotypes presented by our fly models, and we found a genetic link between *Caz* and *ter94*, which is the *Drosophila* ortholog of human *Valosin-containing protein* (*VCP*).

VCP is a member of the AAA (ATPase associated with a variety of cellular activities) family of proteins, which are implicated in a large variety of biological functions including the regulation of ubiquitin-dependent protein degradation, control of membrane fusion and of dynamics of subcellular components, vesicle-mediated transport and nucleocytoplasmic shuttling (22–24). Association of *VCP* mutations with human disease was first identified in patients with IBMPFD (inclusion body myopathy with early-onset Paget disease and frontotemporal dementia) (25) and more recently in those with ALS (26). There is a single ortholog of human *VCP* in *Drosophila,* named *ter94*, which is predicted to share ~83% amino acid sequence identity with human VCP.

Here, we found that genetic crossing the strongest loss-of-function allele of *ter94* with *Caz*-knockdown severely enhanced the *Caz*-knockdown phenotypes in flies; it severely exacerbated locomotive disabilities and the degeneration of MNs induced by neuron-specific *Caz*-knockdown. Conversely, the overexpression of *ter94* rescued those phenotypes.

RESULTS

Knockdown of *Caz* in eye imaginal discs induces morphologically aberrant rough eyes

To investigate the molecular mechanisms of FUS-related neurodegeneration, we have already generated *Caz*-knockdown fly models of ALS by using the highly versatile GAL4/UAS-targeted expression system (19). To eliminate the possibility of off-target effects, we generated 11 independent transgenic fly lines and obtained one fly line from the Vienna *Drosophila* RNAi center (VDRC; Table 1); *Caz* double-stranded RNA (dsRNA; inverted repeats, IRs) targeted to the different region of the *Caz* mRNA is expressed in those fly lines as described in our previous study (19). The RNAi of the fly lines we generated (responder controls) was targeted to the region corresponding to residues 1–167 (four lines, UAS-*Caz*-IR$_{1-167}$) and 180–346 (seven

Table 1. Associated phenotypes of fly strains carrying UAS-Caz-IR crossed with different GAL4 driver strains

	Transgene strain	Chromosome linkage	Act5C-GAL4> 28°C	Act5C-GAL4> 25°C	GMR-GAL4>	elav>GAL4
UAS-*Caz*-IR$_{1-167}$	3	III	Lethal	Lethal		
	4	III	Lethal	NE	Mild rough eye	ND
	11	II	Lethal	NE	Mild rough eye	ND
	21	III	Lethal	NE	Mild rough eye	ND
UAS-*Caz*-IR$_{180-346}$	11	II	NE	NE	Mild rough eye	NE
	12	II	NE	NE	Mild rough eye	NE
	17	II	NE	NE	Mild rough eye	ND
	22	III	NE	ND	Mild rough eye	NE
	24	III	NE	NE	ND	NE
	32	III	NE	ND	Mild rough eye	ND
	33	III	NE	NE	Mild rough eye	ND
UAS-*Caz*-IR$_{363-399}$		II	NE	ND	Mild rough eye	LD

We used two independent Caz-RNAi constructs, UAS-*Caz*-IR$_{1-167}$ and UAS-*Caz*-IR$_{180-346}$, to generate 11 independent transgenic fly lines. UAS-*Caz*-IR$_{363-399}$ was obtained from VDRC. To drive the expression of *Caz* dsRNA in the whole body of the flies, or specifically in the eye imaginal discs or neuronal tissues, we cross UAS-*Caz*-IR flies with *Act5C-GAL4*, *GMR-GAL4* or *elav-GAL4* flies, respectively. Phenotypes associated with the resultant genotypes are summarized. Each transgenic strain shows a consistent phenotype. NE, no effect; ND, not determined; LD, locomotive dysfunction.

Downloaded from http://hmg.oxfordjournals.org/ at NCNP on July 2, 2014

lines, UAS-*Caz*-IR$_{180-346}$) of *Drosophila* Caz, respectively. The RNAi of the fly strain obtained from the VDRC (w; UAS-*Caz*-IR$_{363-399}$; +) was targeted to the region corresponding to residues 363–399 of *Drosophila* Caz (UAS-*Caz*-IR$_{363-399}$).

Reportedly, *Caz* mRNA and Caz protein are enriched in the central nervous system (CNS), and Caz protein is present in eye imaginal discs (27). To efficiently screen for genes that affect the phenotypes caused by *Caz*-knockdown, we generated model flies with eye-specific *Caz*-knockdown. Specific knockdown of *Caz* in eye imaginal discs was achieved by crossing the transgenic flies carrying a UAS-*Caz*-IR, in which *Caz* dsRNA is expressed, with *GMR-GAL4* driver lines (*GMR-GAL4*; UAS-*Caz*-IR/+; +). Phenotypes of those model flies are easily characterized by abnormal rough eye morphology; scanning electron microscope (SEM) images showed fusion of ommatidia and loss of mechanosensory bristles (Fig. 1). Phenotypes of those fly lines carrying each UAS-*Caz*-IR crossed with the *GMR-GAL4* driver strain are summarized in Table 1. Flies carrying *GMR-GAL4*; +; + alone exhibited apparently normal eye morphology (Fig. 1A; *GMR*). Flies carrying *GMR-GAL4*; UAS-*Caz*-IR$_{1-167}$/+; + (GMR>UAS-*Caz*-IR$_{1-167}$) and those carrying *GMR-GAL4*; UAS-*Caz*-IR$_{363-399}$/+; + (GMR>UAS-*Caz*-IR$_{363-399}$) showed essentially the same rough-eye phenotype (Fig. 1B and C). These results demonstrated that the rough-eye phenotype observed in *Caz*-knockdown flies was not due to a possible insertional mutation or off-target effect, but rather to reduced Caz protein levels. Throughout the following studies, we used fly strains carrying UAS-*Caz*-IR$_{363-399}$, and UAS-*Caz*-IR hereafter refers to this fly strain.

Loss-of-function mutations and overexpression of *ter94* conversely modified the compound eye degeneration induced by *Caz*-knockdown

To examine a genetic interaction between *Caz* and ALS-causing genes, we first crossed eye-specific *Caz*-knockdown flies with several fly lines carrying different mutations in various ALS-causing genes, and their progeny were screened for eye phenotypes. From these screens, we detected a genetic interaction between *Caz* and *ter94*, the *Drosophila* ortholog of human *VCP*. We crossed *Caz*-knockdown flies with ethyl methanesulfonate-induced *ter94* mutations, $ter94^{K15502}$ and $ter94^{03775}$. The phenotypic characterization of two P-element alleles of *ter94* mutations was described previously (28). According to this report, female germ-line clones of a strong loss-of-function allele of *ter94*, $ter94^{K15502}$, do not produce germaria or egg chambers, and female germ-line clones of another slightly less strong loss-of-function allele of *ter94*, $ter94^{03775}$, formed germalia which give rise to stage 6 or 7 egg chambers before degeneration occurs (28). From these findings, we used the $ter94^{K15502}$ mutation as a strongest loss-of-function allele and the $ter94^{03775}$ mutation as a strong loss-of-function allele. The strongest ($ter94^{K15502}$) and strong ($ter94^{03775}$) loss-of-function mutations in the heterozygous states remarkably enhanced the rough-eye phenotype induced by eye-specific *Caz*-knockdown GMR>UAS-*Caz*-IR$_{363-399}$/$ter94^{K15502}$ (Fig. 1D) and GMR>UAS-*Caz*-IR$_{363-399}$/$ter94^{03775}$ (Fig. 1E), respectively. The progeny of eye-specific *Caz*-knockdown flies became lethal at the pupal stage when crossed with *ter94*-knockdown or a chromosomal deficiency line: *Df (2R) X1* lacking the genomic region 46C2-47A01 that contains *ter94*. These results indicate that loss-of-function mutations of *ter94* act as dominant enhancers of the *Caz*-knockdown-induced rough-eye phenotype. Conversely, the overexpression of wild-type *ter94* (GMR>UAS-*Caz*-IR$_{363-399}$/UAS-*ter94*) obviously suppressed the rough-eye phenotype induced by eye-specific *Caz*-knockdown (Fig. 1G) based on a comparison with the responder control of UAS-*ter94* flies (GMR>UAS-*Caz*-IR$_{363-399}$/UAS-*GFP*) (Fig. 1F).

Loss-of-function mutation and overexpression of *ter94* had opposite effects on nuclear Caz signals in the larval CNS

We demonstrated in our previous paper that *Drosophila* Caz was strongly expressed in the CNS of third instar larvae and localized in the nucleus (19). Therefore, we investigated whether neuron-specific *Caz*-knockdown changed the expression or subcellular localization of Caz or both; specifically, we crossed fly lines carrying UAS-*Caz*-IR with *elav-GAL4* driver lines. To monitor Caz expression and localization, we immunostained brain-ventral ganglia complexes (BVGCs) of third instar larvae with anti-Caz antibody, which was developed previously (19), and quantified the immunofluorescent signals. The BVGCs of the control larvae, which carried w; +; *elav-GAL4*/+ (*elav*/+), exhibited ubiquitous signals of endogenous Caz (Fig. 2, a driver control, A1), but the signal intensity of endogenous Caz in the BVGCs was remarkably reduced in neuron-specific *Caz*-knockdown larvae carrying UAS-*Caz*-IR/+; *elav-GAL4*/+ (Fig. 2, elav>UAS-*Caz*-IR, C1). In driver control larvae, anti-Caz immunoreactivity was evident in the nucleus of the neuronal cells, but it did not colocalize with actin filaments stained with phalloidin (Fig. 2, B1, B2, B1+B2) or with chromosomes stained with diamino-2-phenylidole (DAPI; Fig. 2, B1, B3, B1+B3). These findings indicated that Caz must localize in the nucleoplasm. The intensity of nuclear Caz signals was significantly reduced in the BVGCs of neuron-specific *Caz*-knockdown larvae carrying elav>UAS-*Caz*-IR [intensity units = 8.89 (arbitrary units), measured in Fig. 2, D1] compared with that of driver control larvae (intensity units = 31.5, measured in Fig. 2, B1; $P < 0.001$, Fig. 2G).

Next, we examined the effects of ter94 on neuron-specific *Caz*-knockdown with regard to Caz levels and localization. First, we examined Caz expression and localization in larvae carrying a heterozygous loss-of-function *ter94* mutation and neuron-specific *Caz*-knockdown constructs. Larvae carrying the strongest loss-of-function allele of *ter94* and neuron-specific *Caz*-knockdown, UAS-*Caz*-IR/ $ter94^{K15502}$; *elav-GAL4*/+ (Fig. 2, elav>UAS-*Caz*-IR/$ter94^{K15502}$, E1) exhibited remarkably reduced Caz signals in the BVGCs when compared with UAS-*Caz*-IR/+; *elav-GAL4*/+ larvae. The intensity of nuclear Caz signal was significantly reduced in these larvae carrying elav>UAS-*Caz*-IR/$ter94^{K15502}$ (intensity units = 6.68, measured in Fig. 2, F1), even compared with that of the larvae carrying elav>UAS-*Caz*-IR (Fig. 2, D1) ($P < 0.05$, Fig. 2G). These results indicated that neuron-specific *Caz*-knockdown significantly reduced nuclear Caz expression, and this reduction was enhanced by genetic crossing with the strongest loss-of-function allele of *ter94*.

Conversely, compared with the Caz signals in BVGCs of larvae carrying UAS-*Caz*-IR/UAS-*GFP*; *elav-GAL4*/+ (Fig. 3, elav>UAS-*Caz*-IR/UAS-*GFP*, A1), Caz signals in

Downloaded from http://hmg.oxfordjournals.org/ at NCNP on July 2, 2014

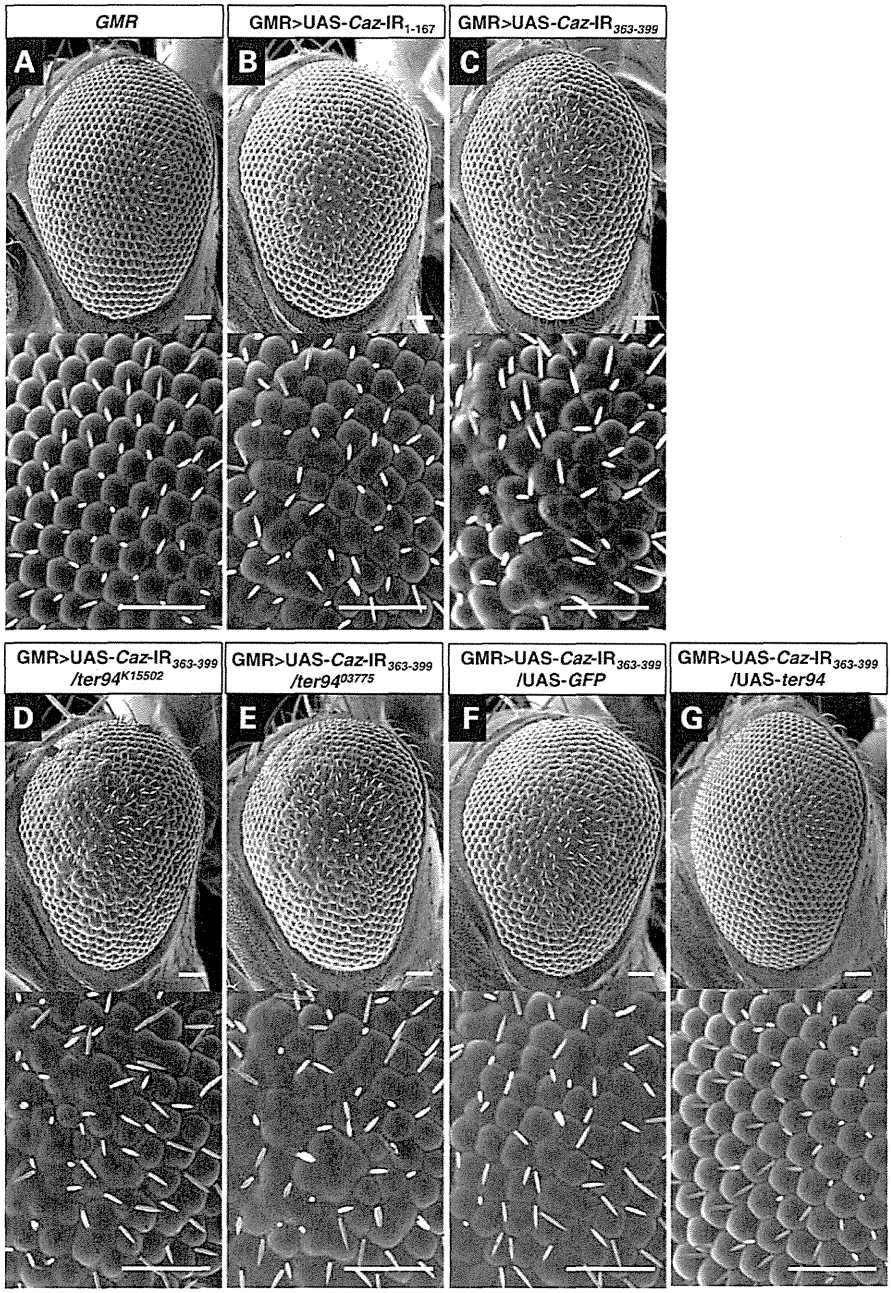

Figure 1. The rough-eye phenotype induced by *Caz*-knockdown is modified by genetic changes in *ter94*. Each panel shows a scanning electron micrograph of the compound eye of a 3-day-old adult fly. Each lower panel is a higher magnification image of the corresponding upper panel. Specific knockdown of *Caz* in eye imaginal discs was achieved by crossing the transgenic flies that carried UAS-*Caz*-IR with the *GMR-GAL4* driver. (**A**) The eyes of a control fly carrying *GMR-GAL4*; +; + (*GMR*) exhibit apparently normal eye morphology having an organized ommatidial architecture. (**B** and **C**) Adult eyes from two independent fly lines with eye-specific *Caz*-knockdown. Flies from line with UAS-*Caz*-IR1–167 (strain 4, Table 1) or from the line with UAS-*Caz*-IR363–399 were crossed with flies from the *GMR-GAL4* driver strain. Resultant flies carrying GMR>UAS-*Caz*-IR1–167 (B) or GMR>UAS-*Caz*-IR363–399 (C) have essentially the same rough-eye phenotype and exhibit ommatidial degeneration. (**D** and **E**) Adult eyes from two independent fly lines; each line has eye-specific *Caz*-knockdown and a distinct loss-of-function mutation in *ter94*. The eye-specific *Caz*-knockdown fly line (GMR>UAS-*Caz*-IR363–399/UAS-*Caz*-IR363–399) was crossed with flies carrying the strongest ($ter94^{K15502}$) or a strong ($ter94^{03775}$) loss-of-function *ter94* mutation. The resultant flies carrying GMR>UAS-*Caz*-IR363–399/$ter94^{K15502}$ (D) or GMR>UAS-*Caz*-IR363–399/$ter94^{03775}$ (E) show rough-eye phenotypes that is enhanced relative to that observed in flies with GMR>UAS-*Caz*-IR363–399 alone (C). Adult eyes from fly lines resulting from crosses of eye-specific *Caz*-knockdown flies with UAS-*GFP* (GMR>UAS-*Caz*-IR363–399/UAS-*GFP*, a responder control, **F**) or UAS-*ter94* (GMR>UAS-*Caz*-IR363–399/UAS-*ter94*, **G**). The rough-eye phenotype induced by eye-specific *Caz*-knockdown is obviously less severe in the presence of UAS-*ter94* (G) than in the presence of UAS-*GFP* (F). Posterior is to the right, and dorsal is to the top. The flies were developed at 28°C. Scale bars indicate 50 μm.

Downloaded from http://hmg.oxfordjournals.org/ at NCNP on July 2, 2014

BVGCs were remarkably stronger in larvae carrying UAS-*Caz*-IR/ UAS-*ter94*; *elav-GAL4*/+, in which wild-type *ter94* was overexpressed under the *Caz*-knockdown background (Fig. 3, elav>UAS-*Caz*-IR/UAS-*ter94*, C1). Quantification of the Caz signal revealed that the intensity of nuclear Caz signal was 3.69-fold higher in elav>UAS-*Caz*-IR/UAS-*ter94* larvae (intensity units = 23.5, measured in Fig. 3, D1) than in elav> UAS-*Caz*-IR/UAS-*GFP* larvae (intensity units = 6.36, measured in Fig. 3, B1; $P < 0.001$, Fig. 3E). These results indicated that overexpression of wild-type *ter94* restored the reduced Caz signal in the nucleus induced by neuron-specific *Caz*-knockdown. Taken together, our presented results suggest that ter94 levels could enhance or rescue the Caz-knockdown phenotype.

To clarify whether or not altered ter94 protein levels affect the knock-down machinery, we carried out immunoblot analyses of CNS extracts of third instar larvae carrying *elav*/+, elav>UAS-*Caz*-IR, elav>UAS-*Caz*-IR/*ter94* ^{K15502}, elav>UAS-*Caz*-IR/UAS-*GFP* and elav>UAS-*Caz*-IR/UAS-*ter94*. A single major band with an apparent molecular weight of 45 kDa was detected on immunoblots of all the flies using the anti-Caz antibody (Supplementary Material, Fig. S1A). The intensity of this Caz protein band was apparently reduced in larvae carrying elav>UAS-*Caz*-IR compared with its intensity in larvae carrying *elav*/+ (Supplementary Material, Fig. S1A and B). We then found that there was no apparent difference in Caz protein levels of CNS extracts either between the larvae carrying elav>UAS-*Caz*-IR and elav>UAS-*Caz*-IR/ *ter94*^{K15502} or between the larvae carrying elav>UAS-*Caz*-IR/UAS-*GFP* and elav>UAS-*Caz*-IR/UAS-*ter94* (Supplementary Material, Fig. S1A and B). These results suggest that ter94 levels do not affect the Caz protein level on *Caz*-knockdown larvae, but indeed decrease or restore nuclear Caz protein levels in *Caz*-knockdown larvae.

Effects of a loss-of-function mutation and of overexpression of *ter94* on the mobility defects caused by neuron-specific *Caz*-knockdown

Because ALS is an age-related motor neuron disease, we examined the effect of neuron-specific *Caz*-knockdown on the locomotive function of adult flies of different ages by using a well-established climbing assay (29). We also examined the effects of loss-of-function or overexpression of *ter94* on changes in climbing ability caused by neuron-specific *Caz*-knockdown. All the fly strains showed an age-dependent decline in the climbing ability (Fig. 4). Neuron-specific *Caz*-knockdown flies carrying elav>UAS-*Caz*-IR exhibited a significantly decreased climbing ability at the following days of age; day 7, −10.4%; and day 21, −16.8%, $P < 0.001$; day 14, −10.6%, $P < 0.01$; day 28, −14.7%, $P < 0.05$ (Fig. 4A, gray columns). Flies carrying the strongest loss-of-function allele of *ter94* and neuron-specific *Caz*-knockdown (elav>UAS-*Caz*-IR/*ter94*^{K15502}) had significantly worse locomotive ability than did flies with neuron-specific *Caz*-knockdown alone (elav>UAS-*Caz*-IR) for every age examined (day 3, −14.0%; day 7, −19.5%; day 14, −35.2%; day 21, −49.7%; day 28, −63%; $P < 0.001$, Fig. 4A, black columns). Conversely, flies that overexpressed wild-type *ter94* in the background of neuron-specific *Caz*-knockdown (elav>UAS-*Caz*-IR/UAS-*ter94*) had significantly better climbing ability than did control flies with neuron-specific *Caz*-knockdown (elav>UAS-*Caz*-IR/UAS-*GFP*) until day 14 (day 3, +24.8%; day 14, +21.8%, $P < 0.001$; day 7, +15.5%, $P < 0.01$; Fig. 4B, black columns), but not after that (day 21, not significant, $P = 0.98$; day 28, reduced climbing ability, −37.4%, $P < 0.01$; Fig. 4B, black columns). There were no significant differences in climbing abilities among *elav*/+ (a driver control), UAS-*Caz*-IR/+ (a responder control) and *ter94* ^{K15502}/+ flies in each day after exclusion that was monitored until 14 days (Supplementary Material, Fig. S2). Flies carrying elav>UAS-*Caz*-IR/UAS-*GFP* exhibited a significantly decreased climbing ability for every age examined (day 3, −32.8%; day 7, −23.8%; day14, −26.1%; day 21, −42.4%; day 28, −47.9%, $P < 0.001$; Fig. 4B, gray columns) compared with those carrying *elav*/+ (Fig. 4B, white columns). Until day 3, the climbing ability of flies carrying elav>UAS-*Caz*-IR/UAS-*ter94* was recovered almost as well as that of flies carrying *elav*/+. However, that of flies carrying elav>UAS-*Caz*-IR/UAS-*ter94* was not fully recovered, and significantly less than that of those carrying *elav*/+ after day 3 at the following days of age; day 7, −12.8%; day 21, −42.4%; day 28, −27.8%, $P < 0.001$; day 14, −10.0%, $P < 0.01$ (Fig. 4B, black columns) compared with those carrying *elav*/+ (Fig. 4B, white columns). Together, our data demonstrate that neuron-specific *Caz*-knockdown leads to a severe progressive locomotive defect in adult flies, and that overexpression of wild-type *ter94* could rescue the locomotive defect until certain fly ages, whereas loss of *ter94* function significantly exacerbated this *Caz*-knockdown defect throughout the adult life span of these flies. We next examined the fly life span of the fly models with neuron-specific *Caz*-knockdown and genetically modified *ter94*. There were no significant differences in life spans among the control flies carrying *elav*/+ (the average life span = 50.9 days, $n = 151$), neuron-specific *Caz*-knockdown flies carrying elav>UAS-*Caz*-IR (48.3 days, $n = 123$), and flies carrying the strongest loss-of-function allele of *ter94* and neuron-specific *Caz*-knockdown (elav> UAS-*Caz*-IR/*ter94*^{K15502}, 47.5 days, $n = 120$) (Supplementary Material, Fig. S3A). Similarly, there were no significant differences in life spans between neuron-specific *Caz*-knockdown flies carrying elav>UAS-*Caz*-IR/UAS-*GFP* (responder control, the average life span = 44.8 days, $n = 140$) and those carrying *ter94* overexpression in the background of neuron-specific *Caz*-knockdown, elav>UAS-*Caz*-IR/UAS-*ter94* (41.1 days, $n = 140$) (Supplementary Material, Fig. S3B). In our Caz-knockdown fly models, the expression of Caz protein was decreased to 40–60% in the CNS, but their life spans were not reduced (19). These results suggest that the substantial expression of Caz in neuronal tissues, even though it is not fully expressed, could sufficiently keep their life spans within normal range.

The effects of loss-of-function mutation and overexpression of *ter94* on the morphology of MN presynaptic terminals in the NMJs of neuron-specific *Caz*-knockdown flies

Based on the finding that our *Caz*-knockdown flies showed motor deficits in the climbing assay (19) and the fact that *FUS*, the human ortholog of *Caz*, is involved in ALS that impairs motor neurons, we analyzed the morphology of MN presynaptic

Downloaded from http://hmg.oxfordjournals.org/ at NCNP on July 2, 2014

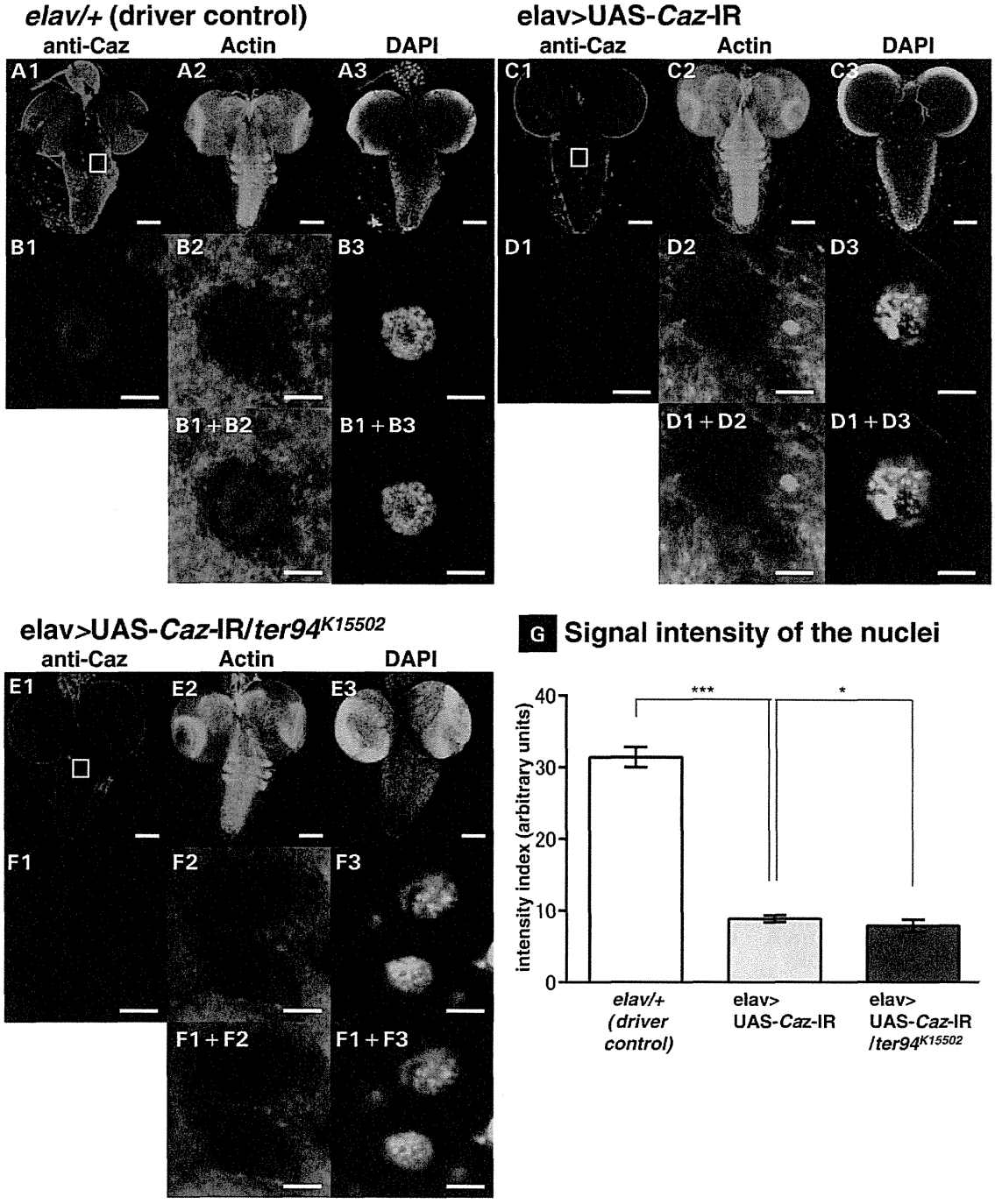

Figure 2. Neuron-specific *Caz*-knockdown reduces Caz signal in nuclei within larval CNS, and this reduction is significantly exacerbated by a loss-of-function *ter94* mutation. **(A)**–**(F)** are representative images of corresponding genotypes. (A1)–(A3) are immunofluorescent images of larval CNS, which comprises BVGC, taken from a driver control larva carrying *elav/+*. (C1)–(C3) are the BVGCs of a *Caz*-knockdown larva carrying UAS-*Caz*-IR. (E1)–(E3) are the BVGCs of a larva co-expressed with $ter94^{K15502}$ in the background of *Caz*-knockdown carrying elav>UAS-*Caz*-IR/$ter94^{K15502}$. (B1)–(B3), (D1)–(D3) and (F1)–(F3) are higher magnification images of the boxed area in (A1), (C1) and (E1), respectively. (B1+B2), (B1+B3), (D1+D2), (D1+D3), (F1+F2) and (F1+F3) are merged images. The indirect immunofluorescence in A1, B1, C1, D1, E1 and F1 is signal from the polyclonal anti-Caz antibody. The fluorescence in A2, B2, C2, D2, E2 and F2 is from phalloidin, which labels actin; the fluorescence in A3, B3, C3, D3, E3 and F3 is from DAPI, which labels DNA. The BVGC of driver control larvae carrying *elav/+* show ubiquitous signals from endogenous Caz (A1), but the signal intensity from endogenous Caz in the BVGC is remarkably reduced in larvae carrying elav>UAS-*Caz*-IR (C1). Anti-Caz antibody immunoreactivity is evident in the nuclei of neuronal cells (B1) and does not colocalize with phalloidin-stained actin filaments (B2, B1+B2). Caz does not colocalize with DAPI (B3, B1+B3). The intensity of nuclear Caz signal is significantly reduced in the BVGCs of larvae carrying

Downloaded from http://hmg.oxfordjournals.org/ at NCNP on July 2, 2014

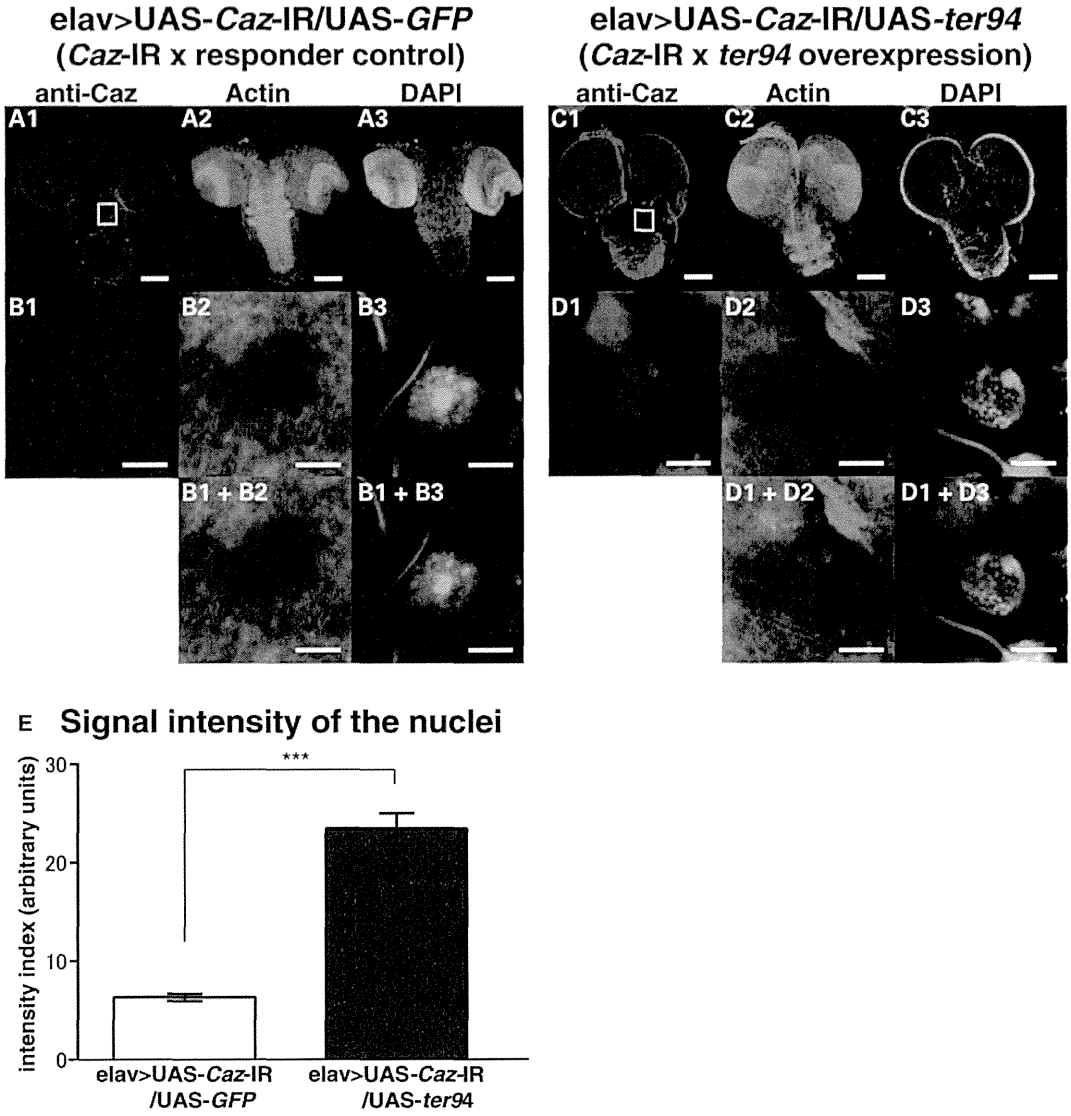

Figure 3. Overexpression of wild-type *ter94* restores Caz signal in nuclei in the CNS of larvae with neuron-specific *Caz*-knockdown. (**A**)–(**D**) are representative images of corresponding genotypes. (A1)–(A3) are the BVGCs of a *Caz*-knockdown larva carrying elav>UAS-*Caz*-IR/UAS-*GFP*. (C1)–(C3) are the BVGCs of a larva that overexpressed wild-type *ter94* in the background of *Caz*-knockdown carrying elav>UAS-*Caz*-IR/UAS-*ter94*. (B1)–(B3) and (D1)–(D3) are higher magnification images of the boxed area in A1 and C1, respectively. (B1+B2), (B1+B3), (D1+D2) and (D1+D3) are merged images. The indirect immunofluorescence in A1, B1, C1 and D1 is the signal from the polyclonal anti-Caz antibody. The fluorescence in A2, B2, C2 and D2 and that in A3, B3, C3 and D3 are from phalloidin and DAPI, respectively. (**E**) shows the mean (± SE) of the intensity of the nuclear Caz signal in the BVGC tissues from the third instar larvae as fluorescence emission in arbitrary units. Columns and horizontal bars show the mean and SE of 15 nuclei, respectively. $^{***}P < 0.001$. Compared with the Caz signals in the BVGCs of the larvae carrying elav>UAS-*Caz*-IR/UAS-*GFP* (A1), Caz signals are remarkably stronger in the BVGCs of the larvae carrying elav>UAS-*Caz*-IR/UAS-*ter94* (C1). The intensity of the nuclear Caz signal is significantly higher in these larvae due to the overexpression of *ter94* (D1) than in the larvae carrying elav>UAS-*Caz*-IR/UAS-*GFP* (B1) ($P < 0.001$, E). The scale bars indicate 100 μm (A1–A3 and C1–C3) and 5 μm (B1–B3 and D1–D3).

elav>UAS-*Caz*-IR (D1) compared with that of driver control larvae (B1) ($P < 0.001$, G). The larvae carrying the strongest loss-of-function allele of *ter94* and neuron-specific *Caz*-knockdown (elav>UAS-*Caz*-IR/*ter94*^{K15502}) (E1) also show remarkably reduced Caz signals in the BVGCs. The intensity of the nuclear Caz signal is significantly reduced in these larvae with the strongest loss-of-function allele of *ter94* and *Caz*-knockdown (F1), even compared with that of the *Caz*-knockdown larvae (D1) ($P < 0.05$, **G**). The scale bars indicate 100 μm (A1–A3, C1–C3 and E1–E3) and 5 μm (B1–B3, D1–D3 and F1–F3). (G) This graph plots the mean (± SE) of the intensity of the nuclear Caz signal in BVGCs from third instar larvae as fluorescence emission in arbitrary units with respect to the genotype; Columns and horizontal bars show the mean and SE of 15 nuclei, respectively. $^{***}P < 0.001$, $^{*}P < 0.05$.

Downloaded from http://hmg.oxfordjournals.org/ at NCNP on July 2, 2014

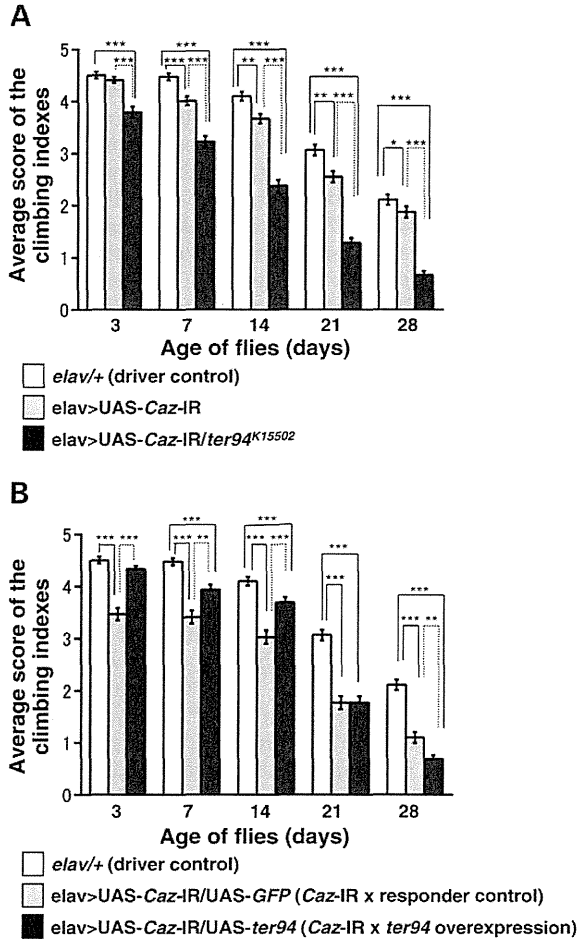

Figure 4. A loss-of-function *ter94* mutation and wild-type *ter94* overexpression have opposite effects on the climbing ability of neuron-specific *Caz*-knockdown flies. (**A**) The locomotive ability of driver control flies, which carrying *elav/+* ($n = 366$, white columns), is significantly better than that of neuron-specific *Caz*-knockdown flies, which carrying elav>UAS-*Caz*-IR ($n = 296$, gray columns) for every age examined other than day 3. On each day after eclosion that was monitored, adult flies carrying elav>UAS-*Caz*-IR/*ter94*^{K15502} ($n = 210$, black columns) exhibited significantly worse climbing ability than flies carrying neuron-specific *Caz*-knockdown alone. (**B**) Conversely, adult flies carrying elav>UAS-*Caz*-IR/UAS-*ter94* ($n = 215$, black columns) have significantly better climbing ability than flies carrying elav>UAS-*Caz*-IR/UAS-*GFP* ($n = 190$, gray columns) on days 3, 7 and 14, but not after day 14. The climbing ability of flies carrying *elav/+* ($n = 366$, white columns) is significantly better than those carrying elav>UAS-*Caz*-IR/UAS-*GFP* for every age examined, same as those in (A). Until day 3, the climbing ability of flies carrying elav>UAS-*Caz*-IR/UAS-*ter94* is recovered almost as well as that of flies carrying *elav/+*. However, that of the flies carrying elav>UAS-*Caz*-IR/UAS-*ter94* is significantly less than that of flies carrying *elav/+* after day 3. Columns and horizontal bars show the mean and SE of the measurements, respectively. $^{***}P < 0.001$, $^{**}P < 0.01$ and $^{*}P < 0.05$.

terminals at NMJs in *Caz*-knockdown flies. Abnormal NMJ morphology and behavioral defects have been implicated in many *Drosophila* models of neurodegenerative diseases that involve motor disturbances such as spinal muscular atrophy and tauopathies (30,31). Because most MNs of the adult fly originate from larval MNs, we examined the NMJ structure in the larvae from *Caz*-knockdown strains. Previously, we demonstrated that neuron-specific *Caz*-knockdown shortened terminal branches of larval MNs (19). To clarify the effects of the *ter94* mutation on the morphology of MN terminals, we examined the NMJ structure of our *Caz*-knockdown flies with or without *ter94* mutation and with or without wild-type *ter94* overexpression.

Compared with the total length of synaptic branches of MNs in driver control larvae carrying *elav/+* (94.4 ± 8.0 μm, Fig. 5A), which was significantly decreased in neuron-specific *Caz*-knockdown larvae carrying elav>UAS-*Caz*-IR (53.8 ± 6.0 μm, Fig. 5B; $P < 0.001$, Fig. 5D). Furthermore, this decreased branch length caused by neuron-specific *Caz*-knockdown was significantly enhanced by genetic crossing with the strongest loss-of-function allele of *ter94* (elav>UAS-*Caz*-IR/*ter94*^{K15502}, 39.5 ± 1.7 μm, Fig. 5C; $P = 0.035$, Fig. 5D). The average number of synaptic boutons per MN was also significantly smaller in neuron-specific *Caz*-knockdown larvae (9.7 ± 0.5, Fig. 5B) than in control larvae (14.7 ± 1.0, Fig. 5A; $P < 0.001$, Fig. 5E). This decrease in the number of synaptic boutons in the neuron-specific *Caz*-knockdown larvae was significantly enhanced by genetic crossing with the strongest loss-of-function allele of *ter94* (6.5 ± 0.5, Fig. 5C; $P < 0.001$, Fig. 5E). However, there were no significant differences in the size of synaptic boutons among these genotypes (Fig. 5F).

Conversely, the total branch length was significantly longer in the larvae with *ter94* overexpression in the background of neuron-specific *Caz*-knockdown (elav>UAS-*Caz*-IR/UAS-*ter94*, Fig. 5H and I) than in responder control larvae (elav>UAS-*Caz*-IR/UAS-*GFP*, Fig. 5G; 110.7 ± 12.0 versus 54.7 ± 2.5 μm, $P < 0.001$, Fig. 5J). The total branch length in the larvae carrying elav>UAS-*Caz*-IR/UAS-*GFP* was also significantly decreased compared with those carrying *elav/+* (94.4 ± 8.0 versus 54.7 ± 2.5 μm, $P < 0.001$, Fig. 5J). However, there were no significant differences about the total branch length between the larvae carrying *elav/+* and elav>UAS-*Caz*-IR/UAS-*ter94* (Fig. 5J). These results indicated that a loss-of-function *ter94* mutation and wild-type *ter94* overexpression have opposite effects on the synaptic terminal growth and morphogenesis that is impaired by *Caz*-knockdown. Notably, in the larvae with *ter94* overexpression in the background of neuron-specific *Caz*-knockdown (elav>UAS-*Caz*-IR/UAS-t*er94*), the extent of increase in the total branch length showed considerable variability (Fig. 5H and I). Of the larvae with *ter94* overexpression in the background of neuron-specific *Caz*-knockdown, 28% had branch lengths (Fig. 5I) that were 2-fold or more elongated relative to the responder controls (Fig. 5G). The larvae carrying elav>UAS-*Caz*-IR/UAS-*ter94* (Fig. 5H and I) also showed significantly increased number of synaptic boutons of MN terminals (25.6 ± 3.5) compared with those carrying elav>UAS-*Caz*-IR/UAS-*GFP* (8.7 ± 0.5, Fig. 5G; $P < 0.001$, Fig. 5K). The number of synaptic boutons in the larvae carrying elav>UAS-*Caz*-IR/UAS-*GFP* was also significantly decreased compared with that of those carrying *elav/+* (8.7 ± 0.5 versus 14.7 ± 1.0, $P < 0.01$, Fig. 5K). The number of synaptic boutons in the larvae carrying elav>UAS-*Caz*-IR/UAS-*ter94* was significantly increased compared with that of those carrying *elav/+* (14.7 ± 1.0 versus 25.6 ± 3.5, $P < 0.05$, Fig. 5K). The number of synaptic boutons of MNs might be increased in

Downloaded from http://hmg.oxfordjournals.org/ at NCNP on July 2, 2014

the larvae carrying elav>UAS-*Caz*-IR/UAS-*ter94* due to the growth of synaptic terminals. There were no significant differences in the size of synaptic boutons among these genotypes (Fig. 5L). These results indicated that Caz is required for growth of MN terminals and formation of synaptic boutons at the NMJ, and these functions of Caz at the MN terminals are affected by the levels of ter94 protein.

DISCUSSION

Here, we demonstrated that eye-specific and neuron-specific *Caz*-knockdown induced a rough-eye phenotype and locomotive dysfunction, respectively; moreover, the locomotive dysfunction was due to the degeneration of MNs. The strongest loss-of-function allele of *ter94* ($ter94^{k15502}$) enhanced such rough-eye and locomotive-dysfunction phenotypes induced by *Caz*-knockdown. Conversely, the overexpression of wild-type *ter94* significantly suppressed the phenotypes induced by *Caz*-knockdown such as rough-eye phenotype, locomotive disabilities and degeneration of MNs. Moreover, neuron-specific *Caz*-knockdown decreased Caz levels in nuclei, and overexpression of wild-type *ter94* significantly suppressed the effects on nuclear *Caz*-expression levels induced by *Caz*-knockdown.

VCP is a member of the AAA protein family; these proteins are involved in diverse cellular functions and in a variety of physiological processes such as cell cycle regulation, membrane fusion, ER-associated degradation, ubiquitin-mediated protein degradation and nucleocytoplasmic shuttling (22–24). VCP is implicated in various neurodegenerative disorders. Mutations in the human *VCP* gene have been reported to cause frontotemporal dementia associated with IBMPFD or familial ALS, and VCP is consequently now considered as a causative gene for FTLD/ALS (25,26). Additionally, previous studies demonstrated that VCP is a binding partner of polyglutamine (polyQ) disease proteins with expanded polyQ tracts (huntingtin, ataxin-1, ataxin-3, ataxin-7 and androgen receptor) (32,33). Previously, the *Drosophila* ortholog of *VCP*, *ter94*, was identified in a screen for genetic modifiers of the eye degeneration phenotypes induced by eye-specific expression of an expanded polyQ tract (34). Moreover, VCP may be involved in diseases that are caused by changes in protein conformation; notably, VCP has been shown to colocalize with pathological protein aggregates in cases of Parkinson's disease, dementia with Lewy bodies, superoxide dismutase 1-associated ALS and Alzheimer's disease (32,35–37).

Our results demonstrate, for the first time, a genetic link between *Caz* and *ter94*, the *Drosophila* orthologs of *FUS* and *VCP*, respectively. Although it would be necessary to confirm whether that is *Drosophila*-specific or not, our results suggest genetic interaction between *FUS* and *VCP* in human. Genetic interaction between TDP-43 and VCP in *Drosophila* was demonstrated previously; IBMPFD-causing mutations in *ter94* lead to redistribution of TDP-43, from the nucleus to the cytoplasm, and redistribution of TDP-43 is sufficient to induce morphologically aberrant rough eyes (24). This previous report suggests that VCP can balance the amount of TDP-43, which is a constituent of larger heteronuclear ribonucleoprotein (hnRNP) complexes, between nucleus and cytoplasm by acting as a nucleocytoplasmic shuttling molecule (Fig. 6). In this schema, VCP functions to remove TDP-43 from RNP complexes, import TDP-43 into nuclei and degrade TDP-43 via autophagy (24,38,39). VCP might have similar functions with respect to FUS because FUS and TDP-43 have significant structural and functional similarities and are implicated in similar molecular processes (40–42). For example, TDP-43 and FUS act in the context of larger hnRNP complexes. FUS also continuously moves between the nucleus and the cytoplasm (16,17,43,44); therefore, FUS not only regulates gene expression in the nucleus, but also has important functions in the cytoplasm (5). Here, we showed that the decreased level of Caz in the nucleus and the resultant motor disturbance induced by neuron-specific *Caz*-knockdown could be rescued by overexpressed wild-type *ter94* despite lacking any change of Caz protein in the CNS (Supplementary Material, Fig. S1A and B). If VCP has a shuttling function as shown in Figure 6, wild-type ter94 overexpression could translocate Caz from cytoplasm to nucleus because nuclear importing function of ter94 would be dominantly induced in the situation with the deficiency of Caz in the nucleus. Conversely, the loss-of-function allele of *ter94* ($ter94^{k15502}$) exacerbated the depletion of *Caz* from the nucleus probably because ter94-mediated nuclear import of Caz was compromised.

It has been demonstrated that a polyQ tract can interact with VCP in *Drosophila* (34); specifically, either the strongest ($ter94^{k15502}$) or strong ($ter94^{03775}$) loss-of-function allele of *ter94* suppressed the eye degeneration induced by an expanded polyQ tract, whereas the overexpression of wild-type *ter94* in the background of *Caz*-knockdown enhanced this phenotype. Additionally, a chromosomal deletion of 46C3–46E02, the genomic region that contains *ter94*, acted as a dominant suppressor of the polyQ-induced phenotype (34). Our present study and these previous reports together indicate that gain and loss of *ter94* function rescued and exacerbated *Caz*-knockdown phenotypes, respectively, and that they had the converse effects on polyQ-induced phenotypes. These converse effects could be explained by the difference in disease pathogenesis; in polyQ-induced disease models, polyQ-containing pathogenic aggregates exist in nuclei of affected neurons; in contrast, Caz expression in nuclei is deficient in *Caz*-knockdown disease models. Overexpression of wild-type *ter94*, which functions in nuclear import of polyQ or Caz, would exacerbate nuclear polyQ aggregation, but could alleviate the nuclear deficiency of Caz protein.

Neuron-specific *Caz*-knockdown flies showed an age-dependent decline in climbing ability that was significantly worse than driver control flies for every age examined after day 7. Overexpression of wild-type *ter94* significantly rescued the declined locomotor ability caused by *Caz*-knockdown up to day 14, but it did not rescue the phenotype at later stages. Regarding the age-dependent ability to rescue locomotive deficits, we considered the two following possible explanations. First, the elongation of the branch length of MN terminals at NMJs caused by overexpression of wild-type *ter94* in neuron-specific *Caz*-knockdown flies may have alleviated the locomotive defects caused by neuron-specific *Caz*-knockdown. However, the extent of this elongation was highly variable. A previous report showed that larvae with NMJ overgrowth phenotypes exhibited mobility defects; this finding indicates that the elongation of nerve terminal branches beyond some adequate

Downloaded from http://hmg.oxfordjournals.org/ at NCNP on July 2, 2014

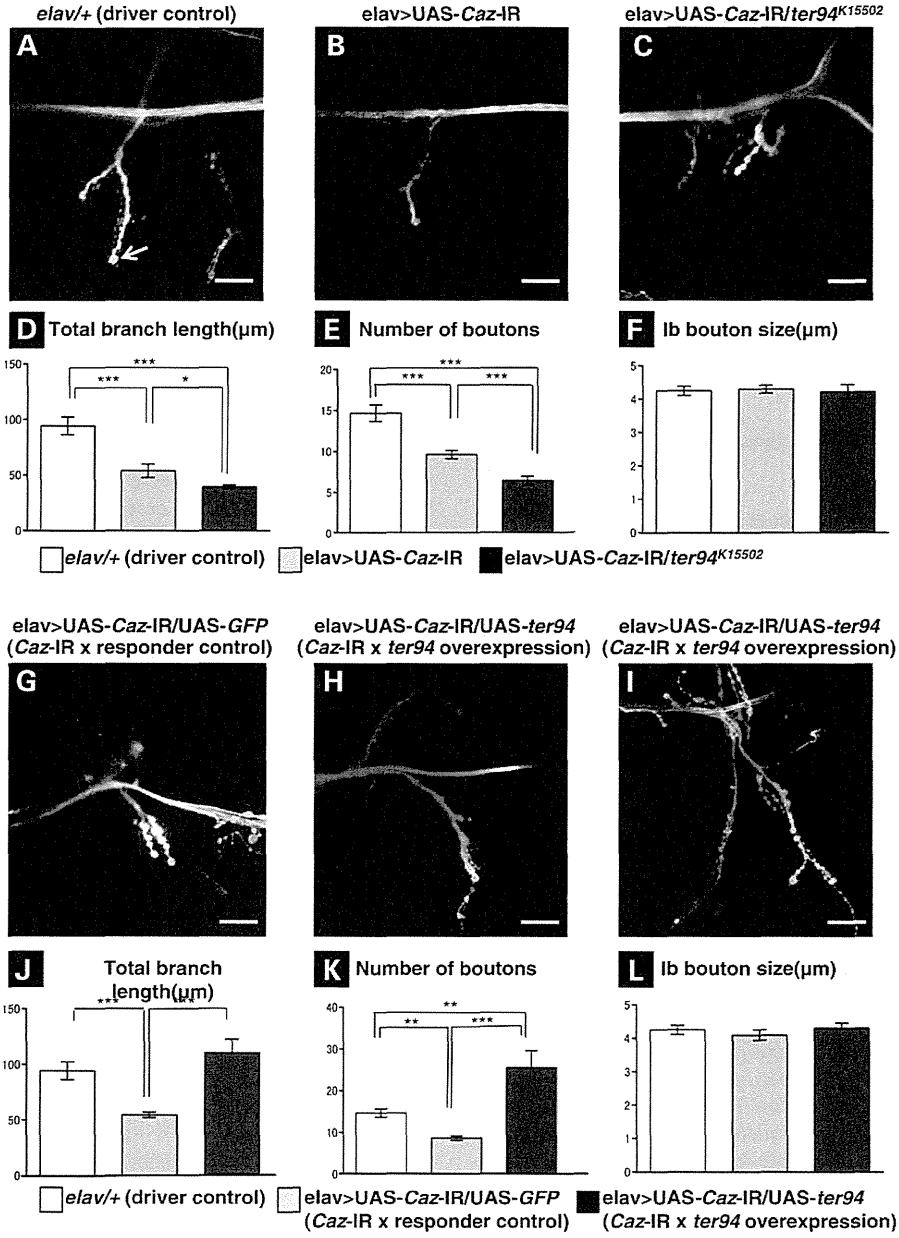

Figure 5. A loss-of-function *ter94* mutation and wild-type *ter94* overexpression change the morphology of MN presynaptic terminals in the NMJ of MN4 in neuron-specific *Caz*-knockdown larvae in opposite ways. A representative image of anti-horseradish peroxidase staining of muscle 4 synapses in third instar larvae with *elav/+* (**A**; a driver control), neuron-specific *Caz*-knockdown (**B**; elav>UAS-*Caz*-IR), neuron-specific *Caz*-knockdown crossed with the strongest loss-of-function mutation of *ter94* (**C**; elav>UAS-*Caz*-IR/*ter94*^{K15502}), neuron-specific *Caz*-knockdown crossed with UAS-*GFP* (**G**; elav>UAS-*Caz*-IR/UAS-*GFP*; a responder control) or neuron-specific *Caz*-knockdown crossed with UAS-*ter94* (**H** and **I**; different larvae with the same genotype, elav>UAS-*Caz*-IR/UAS-*ter94*). (**D** and **J**) Total branch length of the NMJ from muscle 4 for each of the indicated genotypes. Compared with the total length of synaptic branches of MNs in driver control larvae (A), that in neuron-specific *Caz*-knockdown larvae (B) is significantly decreased ($P < 0.001$, $n = 10$, D). This decrease in branch length observed in the neuron-specific *Caz*-knockdown larvae (B) is significantly worsened in larvae carrying the strongest loss-of-function allele of *ter94* and neuron-specific *Caz*-knockdown (C) ($P < 0.05$, $n = 10$, D). Conversely, the total branch length in larvae that overexpressed wild-type *ter94* in the background of neuron-specific *Caz*-knockdown (H and I) is significantly longer than that in larvae carrying elav>UAS-*Caz*-IR/UAS-*GFP* (G) ($P < 0.001$, $n = 14$, J). The extent of increase in the total branch length of elav>UAS-*Caz*-IR/UAS-*ter94* was highly variable among individual flies (H and I). The total branch length of synaptic branches of MNs in the larvae carrying elav>UAS-*Caz*-IR/UAS-*GFP* is significantly decreased compared with that of larvae carrying *elav/+* ($P < 0.001$, $n = 12$, J). (**E** and **K**) The number of synaptic boutons for each of the indicated genotypes. The number of synaptic boutons of MNs in neuron-specific *Caz*-knockdown larvae (B) is also significantly decreased compared with driver control larvae (A) ($P < 0.001$, $n = 10$, E). This decrease in the number of synaptic boutons in the neuron-specific *Caz*-knockdown larvae is significantly worsened in larvae carrying the strongest loss-of-function allele of *ter94* and neuron-specific *Caz*-knockdown (C) ($P < 0.001$, $n = 10$, E). Conversely, the number of synaptic boutons in the larvae carrying wild-type *ter94* overexpression in the background of neuron-specific *Caz*-knockdown (H and I) is significantly higher than that in responder control larvae (G) ($P < 0.001$, $n = 10$, K). Compared with the larvae carrying *elav/+*, the number of synaptic

Downloaded from http://hmg.oxfordjournals.org/ at NCNP on July 2, 2014

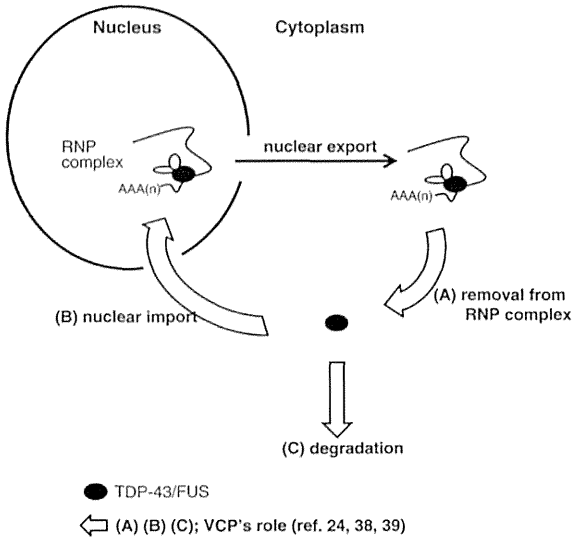

Figure 6. Hypothetical roles of VCP in the nucleoplasmic balance of TDP-43 and FUS referring to the paper by Ritson *et al.* (24). VCP, human ortholog of ter94, may act during removal of TDP-43/FUS from RNP complexes in the cytoplasm (**A**), nuclear import of TDP-43/FUS (**B**) and degradation of TDP-43/FUS by the autophagic pathway (**C**). FUS, the human ortholog of Caz, might translocate from cytoplasm to nucleus when VCP is overexpressed because the nuclear-import function of VCP (B) would be dominantly induced under conditions of FUS deficiency in nuclei. Conversely, loss-of-function alleles of VCP may exacerbate the FUS deficiency in nuclei because FUS is not being properly imported into nuclei by VCP.

length could cause disturbances in locomotive ability (45). Therefore, synaptic MN terminals may have to be within some optimal range of lengths. Second, the age-dependence of ability to rescue the locomotive defects might be due to the age-dependent difference in the expression levels of ter94. Tissue expression data from FlyBase (http://flybase.org) show that mRNA expression levels of *ter94* are very high in the CNS of third instar larvae, but they are relatively low in the head, eye or brain of adults. Age-dependent changes in ter94 expression levels might determine the period within which wild-type ter94 overexpression can rescue locomotive deficits caused by *Caz*-knockdown. Age-dependent effects of ter94 are also evident in fly models of polyQ-induced neurodegeneration. Between the third instar larval stage and the late pupal stage, levels of ter94 were elevated, and elevated levels of ter94 induced severe apoptotic cell death in those pupae (34).

In some IBMPFD-associated VCP mutants, it was previously reported that pathogenic VCPs could bind to cofactors, such as Npl4, Ufd1 or p47, more efficiently than wild-type VCP (46,47). However, little is known about which of the VCP cofactors relate to FUS-nuclear translocation or how the conformational change of VCP affects the interactions of VCP cofactors with other proteins.

In conclusion, we found a genetic interaction between *Caz* and *ter94*. Our data indicate that chemicals that up-regulate the function of VCP or facilitate nuclear import of FUS may suppress the pathogenic processes that lead to the degeneration of MNs in FUS-associated ALS/FTLD. This might be the first step to develop candidate drugs for the disease-modifying therapy of human ALS.

MATERIALS AND METHODS

Fly stocks

Fly stocks were maintained at 25°C on standard food containing 0.7% agar, 5% glucose and 7% dry yeast. Canton S was used as the wild-type strain. The strain: w^{1118}; *P {w [+mC] = UAS-GFP. nls} 14* (DGRC number 107870) (UAS-*GFP*) and chromosomal deficiency line: *Df (2R) X1, Mef2*^{X1}*/CyO, Adh*^{nB} (DGRC number 106718) were obtained from the Kyoto *Drosophila* Genetic Resource Center. The strains: *w* [*]; *P {[+mC] = GAL4-elav.L} 3* (Bloomington BL8760) (*elav-GAL4*), y^1w [*]; *P {[+mC] = Act5C-GAL4} 17bFO1/TM6B, Tb*^{1} (BL3954) (*Act5C-GAL4*), y^1w^{67c23}; *P {w [+mC] = lacW} ter94*^{K15502}*/CyO* (BL10454) (*ter94*^{K15502}) and cn^1P {*ry* [+*t7.2*] = *PZ*} *ter94*^{03775}*/CyO*; *ry*^{506} (BL11349) (*ter94*^{03775}) were obtained from the Bloomington *Drosophila* stock center in Indiana. Establishment of the lines carrying *GMR-GAL4* was as described previously (48). We crossed transgenic UAS-*Caz*-IR flies with *Act5C-GAL4*, *GMR-GAL4* or *elav-GAL4* flies to drive expression of *Caz* dsRNA throughout the whole body of flies, specifically in eye imaginal discs or specifically in neuronal tissues, respectively. We generated eye-specific *Caz*-knockdown flies (*GMR-GAL4*; UAS-*Caz*-IR/+; +) (GMR>UAS-*Caz*-IR) and neuron-specific Caz-knockdown flies (w; UAS-*Caz*-IR/+; *elav-GAL4/+*) (elav>UAS-*Caz*-IR). Each transgenic strain showed a consistent phenotype (Table 1).

Dr Kakizuka kindly provided UAS-*ter94* flies. The UAS-*ter94*-IR strain: w^{1118}; *P {GD9777} v24354* (VDRC number v24354) (*ter94*-knockdown) was obtained from the VDRC. VDRC reports that the *ter94*-RNAi construct is inserted into chromosome 2 and has no off-target effects. The lines generated in this study are as follows: *GMR-GAL4*; +; + (*GMR*), *GMR-GAL4*; UAS-*Caz*-IR363−399/+; + (GMR>UAS-*Caz*-IR), *GMR-GAL4*; UAS-*Caz*-IR363−399/UAS-*Caz*-IR363−399; + (GMR>UAS-*Caz*-IR/UAS-*Caz*-IR), *GMR-GAL4*; UAS-*Caz*-IR363−399/*ter94*^{K15502}; + (GMR>UAS-*Caz*-IR/*ter94*^{K15502}), *GMR-GAL4*; UAS-*Caz*-IR363−399/*ter94*^{03775}; + (GMR>UAS-*Caz*-IR/*ter94*^{03775}), *GMR-GAL4*; UAS-*Caz*-IR363−399/UAS-*GFP*; + (GMR>UAS-*Caz*-IR/UAS-*GFP*), *GMR-GAL4*; UAS-*Caz*-IR363−399/UAS-*ter94*; + (GMR>UAS-*Caz*-IR/UAS-*ter94*), w; +; *elav-GAL4/+* (*elav/+*; a driver control), UAS-*Caz*-IR363−399/+ (UAS-*Caz*-IR/+; a responder control), *ter94*^{K15502}/+, w; UAS-*Caz*-IR363−399/+; *elav-GAL4/+* (elav> UAS-*Caz*-IR), w; UAS-*Caz*-IR363−399/UAS-*Caz*-IR363−399;

boutons is significantly decreased in the larvae carrying elav>UAS-*Caz*-IR/UAS-*GFP* ($P < 0.001$, $n = 10$, K), but significantly increased in those carrying elav> UAS-*Caz*-IR/UAS-*ter94* ($P < 0.05$, $n = 14$, K). (**F** and **L**) The size of synaptic boutons for each of the indicated genotypes. The size of Ib bouton (indicated with an arrow in A) was measured ($n = 31$ for *elav/+*, $n = 33$ for elav>UAS-*Caz*-IR, $n = 31$ for elav>UAS-*Caz*-IR/*ter94*^{K15502}, $n = 30$ for elav>UAS-*Caz*-IR/UAS-*GFP* and $n = 32$ for elav>UAS-*Caz*-IR/UAS-*ter94*). There are no significant differences in the size of synaptic boutons among driver control larvae, either larvae with elav>UAS-*Caz*-IR and those with elav>UAS-*Caz*-IR/*ter94*^{K15502} (F) or among driver control larvae, either larvae with elav>UAS-*Caz*-IR/UAS-*GFP* and elav>

Downloaded from http://hmg.oxfordjournals.org/ at NCNP on July 2, 2014

elav-GAL4/elav-GAL4 (elav>UAS-*Caz*-IR/UAS-*Caz*-IR), w; UAS-*Caz*-IR363–399/*ter94*^{K15502}; *elav-GAL4*/+ (elav>UAS-*Caz*-IR/*ter94*^{K15502}), w; UAS-*Caz*-IR363–399/UAS-*GFP*; *elav-GAL4*/+ (elav>UAS-*Caz*-IR/UAS-*GFP*), w; UAS-*Caz*-IR363–399/UAS-*ter94*; *elav-GAL4*/+ (elav>UAS-*Caz*-IR/UAS-*ter94*).

Immunohistochemistry

Rabbit anti-Caz antibodies were raised against amino acid residues 29–45 and 383–399 of Caz and were produced previously (19). For immunohistochemical analysis, CNS tissues were dissected from third instar larvae and fixed in 4% paraformaldehyde/phosphate buffered saline (PBS) for 15 min at 25°C. These tissue samples were washed with PBS containing 0.3% Triton X-100; fixed samples were then incubated with Alexa 488-conjugated phalloidin (1 unit/200 μl) in PBS containing 0.3% Triton X-100 for 20 min at 25°C. The samples were then blocked with blocking buffer (PBS containing 0.15% Triton X-100 and 10% normal goat serum) for 30 min at 25°C, and then incubated with 1 : 1000 diluted rabbit anti-Caz antibody in the blocking buffer for 20 h at 4°C. After extensive washing with PBS containing 0.3% Triton X-100, samples were incubated in the dark with secondary antibodies labeled with Alexa 546 (1 : 400; Invitrogen) diluted in the blocking buffer for 3 h at 25°C. After washing with PBS containing 0.3% Triton X-100, the samples were stained with DAPI (0.5 μg/ml)/PBS/0.1% Triton X-100. After extensive washing with PBS containing 0.1% Triton X-100 and PBS, the samples were mounted in Vectashield (Vector Laboratories-Inc.) and observed under a confocal laser scanning microscope (OLYMPUS FLUOVIEW FV10i). Images were analyzed with the program MetaMorph Imaging System 7.7 (Molecular Devices Inc.). The use of this program made it possible to quantify the average and the standard error of fluorescence emission from nuclei of each fly strain.

For NMJ staining, third instar larvae were dissected in HL3 saline (49), and then fixed in 4% paraformaldehyde/PBS for 30 min. The blocking buffer contained 2% bovine serum albumin and 0.1% Triton X-100 in PBS. Fluorescein isothiocyanate-conjugated goat anti-horseradish peroxidase (HRP) (1:1000, MP Biochemicals) was used as the detection antibody. The samples were mounted and observed under a confocal laser scanning microscope (Carl Zeiss LSM510, Jena, Germany). MN 4 (Ib) in muscle 4 in abdominal segment 2 was quantified. Images were acquired using a Zeiss LSM 510 confocal laser scanning microscope by merging 1 μm interval z-sections onto a single plane. The MetaMorph imaging system was used to measure nerve terminal branch lengths and Ib bouton sizes.

Immunoblotting analysis

Protein extracts from the CNS of *Drosophila* carrying *elav*/+, elav>UAS-*Caz*-IR, elav>UAS-*Caz*-IR/*ter94* ^{KI5502}, elav>UAS-*Caz*-IR/UAS-*GFP* and elav>UAS-*Caz*-IR/UAS-*ter94* larvae were prepared as described previously (19). Briefly, the CNS was excised from third instar larvae and homogenized in a sample buffer containing 50 mM Tris–HCl (pH 6.8), 2% sodium dodecyl sulfate (SDS), 10% glycerol, 0.1% bromophenol blue and 1.2% β-mercaptoethanol. The homogenates were boiled at 100°C for 5 min and then centrifuged. The supernatants (extracts) were electrophoretically separated on SDS-polyacrylamide gels containing 12% acrylamide and then transferred to polyvinylidene difluoride membranes (Merck, Millipore, MA, USA). The blotted membranes were blocked with tris-buffered saline/0.05% Tween containing 5% skim milk for 1 h at 25°C, followed by incubation with rabbit polyclonal anti-Caz at a 1:5000 dilution for 16 h at 4°C. After washing, the membranes were incubated with HRP-conjugated anti-rabbit IgG (Thermo Scientific, IL, USA) at 1:10 000 dilution for 2 h at 25°C. Antibody binding was detected using ECL Western blotting detection reagents (Thermo Scientific) and images were analyzed using an ImageQuant^{TM} LAS 4000 image analyzer (GE Healthcare Bioscience, Tokyo, Japan). To compare Caz protein levels in the CNS extracts of those larvae, densitometric quantification of the 45-kDa Caz protein bands was carried out. The relative band intensities were quantified and normalized to Coomassie Brilliant Blue staining, then expressed as the percentage of the band intensity derived from larvae carrying *elav*/+.

Scanning electron microscopy

Adult flies were anesthetized with 99% diethyl ether, mounted on stages and observed under an SEM V-7800 (Keyence Inc.) in the low vacuum mode (50). In every experiment, at least five adult flies were chosen from each line for scanning electron microscopy to assess the eye phenotype. For each experiment, there was no significant variation in eye phenotype among the five individuals from the same strain.

Longevity assay

Longevity assays were carried out in a humidified, temperature-controlled incubator set at 25°C and 60% humidity on a 12-h light and 12-h dark cycle; flies were maintained on standard fly food. Flies carrying *elav*/+ ($n = 151$), elav>UAS-*Caz*-IR ($n = 123$), elav>UAS-*Caz*-IR/*ter94*^{K15502} ($n = 120$), elav>UAS-*Caz*-IR/UAS-*GFP* ($n = 140$) or elav>UAS-*Caz*-IR/UAS-*ter94* ($n = 140$) were placed at 28°C, and newly eclosed adult male flies were separated and placed in vials at a low density (20 flies per vial). Every 3 days, they were transferred to new tubes containing fresh food and deaths were scored. The survival rate was determined by plotting a graph of the percentage of surviving flies among total flies at the starting point of each experiment versus days.

Climbing assay

Climbing assays were performed as described previously (29). Flies carrying *elav*/+, UAS-*Caz*-IR/+, *ter94*^{K15502}/+, elav>UAS-*Caz*-IR, elav>UAS-*Caz*-IR/*ter94*^{K15502}, elav>UAS-*Caz*-IR/UAS-*GFP* and elav>UAS-*Caz*-IR/UAS-*ter94* were placed at 28°C, and newly eclosed adult male flies were separated and placed in vials at a density of 20 flies per vial. Flies were transferred, without anesthesia, to a conical tube. The tubes were tapped to collect the flies to the bottom, and they were then given 30 s to climb the wall. After 30 s, the flies were collected at the bottom by tapping of the tube and were again allowed to climb for 30 s. Similar procedures, all of which were videotaped, were repeated five times in total. For each climbing experiment, the height to which each fly

Downloaded from http://hmg.oxfordjournals.org/ at NCNP on July 2, 2014

climbed was scored as score (height climbed); 0 (less than 2 cm), 1 (between 2 and 3.9 cm), 2 (between 4 and 5.9 cm), 3 (between 6 and 7.9 cm), 4 (between 8 and 9.9 cm) or 5 (greater than 10 cm). The climbing index for each fly strain was calculated as follows; each score was multiplied by the number of flies for which that score was recorded, and the products were summed up, then divided by five times the total number of flies examined. These climbing assays were carried out every 7 days until the 28th day after eclosion.

Data analysis

GraphPad Prism version 6.0 was used to perform each statistical analysis. The Mann–Whiney test was used for the assessment of the statistical significance of comparisons between two groups of data. For other assays, one-way analysis of variance (ANOVA) was used to determine the statistical significance of comparisons between groups of data. When the two-way ANOVA showed significant variation among groups, a subsequent Dunnett's test was used for pairwise comparisons between groups. All data are shown as mean ± standard error (SE).

SUPPLEMENTARY MATERIAL

Supplementary Material is available at *HMG* online.

ACKNOWLEDGEMENTS

We would like to thank Dr Kakizuka for generously providing us the UAS-*ter94* fly strains used in these experiments. We would also like to acknowledge Dr H. Yoshida, Ms R. Sahashi, Mr K. Morishita and Mr K. Shimaji for valuable discussion, technical support and suggestions. We thank the Bloomington *Drosophila* stock center, the Vienna *Drosophila* RNAi center and Kyoto *Drosophila* Genetic Resource Center for giving us fly lines.

Conflict of Interest statement. None declared.

FUNDING

This work was supported by Grants-in-Aid from the Research Committee of CNS. Degenerative Diseases, the Ministry of Health, Labour and Welfare of Japan (T.T.), and partly supported by "Integrated Research on Neuropsychiatric Disorders" carried out under the Strategic Research Program for Brain Sciences by the Ministry of Education, Culture, Sports, Science and Technology of Japan (Y.N.). The funders had no role in study design, data collection and analysis, decision to publish or preparation of the manuscript.

REFERENCES

1. Boillée, S., Vande Velde, C. and Cleveland, D.W. (2006) ALS: a disease of motor neurons and their nonneuronal neighbors. *Neuron*, **52**, 39–59.
2. Mackenzie, I.R., Rademakers, R. and Neumann, M. (2010) TDP-43 and FUS in amyotrophic lateral sclerosis and frontotemporal dementia. *Lancet Neurol.*, **9**, 995–1007.
3. Lomen-Hoerth, C., Anderson, T. and Miller, B. (2002) The overlap of amyotrophic lateral sclerosis and frontotemporal dementia. *Neurology*, **59**, 1077–1079.
4. Murphy, J.M., Henry, R.G., Langmore, S., Kramer, J.H., Miller, B.L. and Lomen-Hoerth, C. (2007) Continuum of frontal lobe impairment in amyotrophic lateral sclerosis. *Arch. Neurol.*, **64**, 530–534.
5. Dormann, D. and Haass, C. (2013) Fused in sarcoma (FUS): an oncogene goes awry in neurodegeneration. *Mol. Cell Neurosci.*, **56**, 475–486.
6. Lemmens, R., Moore, M.J., Al-Chalabi, A., Brown, R.H. Jr. and Robberecht, W. (2010) RNA metabolism and the pathogenesis of motor neuron diseases. *Trends Neurosci.*, **33**, 249–258.
7. Gitcho, M.A., Baloh, R.H., Chakraverty, S., Mayo, K., Norton, J.B., Levitch, D., Hatanpaa, K.J., White, C.L. 3rd., Bigio, E.H., Caselli, R. *et al.* (2008) TDP-43 A315 T mutation in familial motor neuron disease. *Ann. Neurol.*, **63**, 535–538.
8. Yokoseki, A., Shiga, A., Tan, C.F., Tagawa, A., Kaneko, H., Koyama, A., Eguchi, H., Tsujino, A., Ikeuchi, T., Kakita, A. *et al.* (2008) TDP-43 mutation in familial amyotrophic lateral sclerosis. *Ann. Neurol.*, **63**, 538–542.
9. Kabashi, E., Valdmanis, P.N., Dion, P., Spiegelman, D., McConkey, B.J., Vande Velde, C., Bouchard, J.P., Lacomblez, L., Pochigaeva, K., Salachas, F. *et al.* (2008) TARDBP mutations in individuals with sporadic and familial amyotrophic lateral sclerosis. *Nat. Genet.*, **40**, 572–574.
10. Sreedharan, J., Blair, I.P., Tripathi, V.B., Hu, X., Vance, C., Rogelj, B., Ackerley, S., Durnall, J.C., Williams, K.L., Buratti, E. *et al.* (2008) TDP-43 mutations in familial and sporadic amyotrophic lateral sclerosis. *Science*, **319**, 1668–1672.
11. Pesiridis, G.S., Lee, V.M. and Trojanowski, J.Q. (2009) Mutations in TDP-43 link glycine-rich domain functions to amyotrophic lateral sclerosis. *Hum. Mol. Genet.*, **18**, R156–R162.
12. Kwiatkowski, T.J. Jr., Bosco, D.A., Leclerc, A.L., Tamrazian, E., Vanderburg, C.R., Russ, C., Davis, A., Gilchrist, J., Kasarskis, E.J., Munsat, T. *et al.* (2009) Mutations in the FUS/TLS gene on chromosome 16 cause familial amyotrophic lateral sclerosis. *Science*, **323**, 1205–1208.
13. Vance, C., Rogelj, B., Hortobágyi, T., De, Vos, K.J., Nishimura, A.L., Sreedharan, J., Hu, X., Smith, B., Ruddy, D., Wright, P. *et al.* (2009) Mutations in FUS, an RNA processing protein, cause familial amyotrophic lateral sclerosis type 6. *Science*, **323**, 1208–1211.
14. Hewitt, C., Kirby, J., Highley, J.R., Hartley, J.A., Hibberd, R., Hollinger, H.C., Williams, T.L., Ince, P.G., McDermott, C.J. and Shaw, P.J. (2010) Novel FUS/TLS mutations and pathology in familial and sporadic amyotrophic lateral sclerosis. *Arch. Neurol.*, **67**, 455–461.
15. Rademakers, R., Stewart, H., Dejesus-Hernandez, M., Krieger, C., Graff-Radford, N., Fabros, M., Briemberg, H., Cashman, N., Eisen, A. and Mackenzie, I.R. (2010) Fus gene mutations in familial and sporadic amyotrophic lateral sclerosis. *Muscle Nerve*, **42**, 170–176.
16. Zinszner, H., Sok, J., Immanuel, D., Yin, Y. and Ron, D. (1997) TLS (FUS) binds RNA in vivo and engages in nucleo-cytoplasmic shuttling. *J. Cell Sci.*, **110**, 1741–1750.
17. Lagier-Tourenne, C., Polymenidou, M. and Cleveland, D.W. (2010) TDP-43 and FUS/TLS: emerging roles in RNA processing and neurodegeneration. *Hum. Mol. Genet.*, **19**, R46–R64.
18. Feiguin, F., Godena, V.K., Romano, G., D'Ambrogio, A., Klima, R. and Baralle, F.E. (2009) Depletion of TDP-43 affects *Drosophila* motoneurons terminal synapsis and locomotive behavior. *FEBS Lett.*, **583**, 1586–1592.
19. Sasayama, H., Shimamura, M., Tokuda, T., Azuma, Y., Yoshida, T., Mizuno, T., Nakagawa, M., Fujikake, N., Nagai, Y. and Yamaguchi, M. (2012) Knockdown of the *Drosophila* fused in sarcoma (FUS) homologue causes deficient locomotive behavior and shortening of motoneuron terminal branches. *PLoS One*, **7**, e39483.
20. Kabashi, E., Bercier, V., Lissouba, A., Liao, M., Brustein, E., Rouleau, G.A. and Drapeau, P. (2011) FUS and TARDBP but not SOD1 interact in genetic models of amyotrophic lateral sclerosis. *PLoS Genet.*, **7**, e1002214.
21. Wang, J.W., Brent, J.R., Tomlinson, A., Shneider, N.A. and McCabe, B.D. (2011) The ALS-associated proteins FUS and TDP-43 function together to affect *Drosophila* locomotion and life span. *J. Clin. Invest.*, **121**, 4118–4126.
22. Meyer, H., Bug, M. and Bremer, S. (2012) Emerging functions of the VCP/p97 AAA-ATPase in the ubiquitin system. *Nat. Cell Biol.*, **14**, 117–123.
23. Braun, R.J. and Zischka, H. (2008) Mechanisms of Cdc48/VCP-mediated cell death: from yeast apoptosis to human disease. *Biochim. Biophys. Acta*, **1783**, 1418–1435.

Downloaded from http://hmg.oxfordjournals.org/ at NCNP on July 2, 2014